Mechanoresponsive regulation of myogenesis by the force-sensing transcriptional regulator Tono

Xu Zhang, Jerome Avellaneda, Maria L Spletter, Sandra B Lemke, Pierre Mangeol, Bianca Habermann, Frank Schnorrer

Article

Current Biology

Mechanoresponsive regulation of myogenesis by the force-sensing transcriptional regulator Tono

Graphical abstract

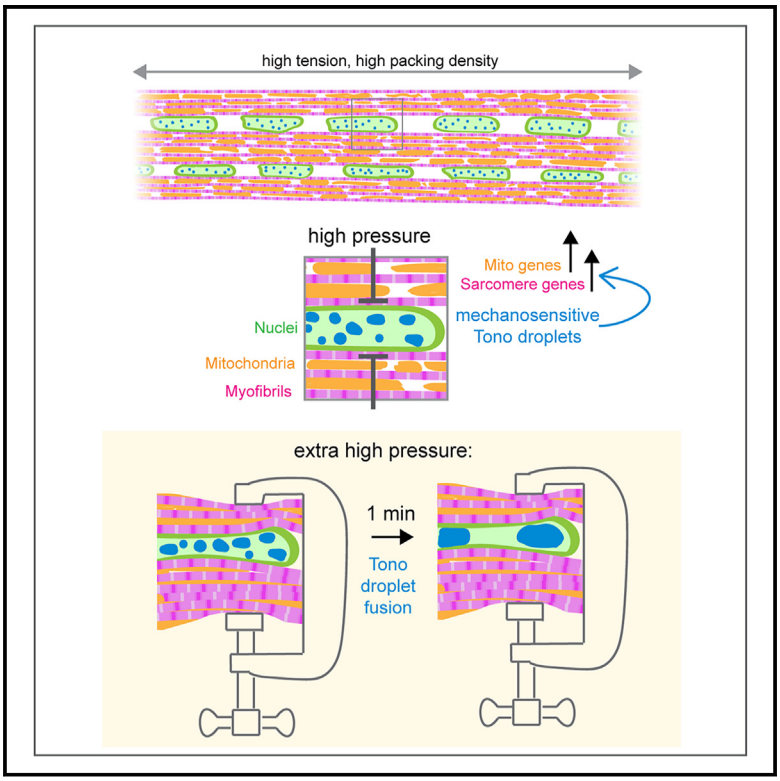

Highlights

- The BTB-zinc-finger protein Tono is a muscle-specific transcriptional regulator
- Tono is required for myofibril and mitochondria maturation during muscle development
- Tono is a mechanosensitive protein that forms droplets upon mechanical pressure
- Growing myofibrils and mitochondria build pressure on muscle nuclei that Tono senses

Authors

Xu Zhang, Jerome Avellaneda, Maria L. Spletter, Sandra B. Lemke, Pierre Mangeol, Bianca H. Habermann, Frank Schnorrer

Correspondence

frank.schnorrer@univ-amu.fr

In brief

Zhang, Avellaneda, et al. identify the BTB-zinc-finger protein Tono as a mechanosensitive transcriptional regulator during flight muscle development in *Drosophila*. After sarcomere assembly, high compressive forces on the muscle nuclei are sensed by Tono to induce a transcriptional transition that triggers sarcomere and mitochondria maturation.

Zhang et al., 2024, Current Biology *34*, 4143–4159
September 23, 2024
https://doi.org/10.1016/j.cub.2024.07.079

CellPress

Current Biology

CellPress
OPEN ACCESS

Article

Mechanoresponsive regulation of myogenesis by the force-sensing transcriptional regulator Tono

Xu Zhang,[1,2,3,6] Jerome Avellaneda,[1,6] Maria L. Spletter,[2,4,5] Sandra B. Lemke,[2] Pierre Mangeol,[1] Bianca H. Habermann,[1,2] and Frank Schnorrer[1,2,7,8,*]

[1]Aix Marseille University, CNRS, IBDM, Turing Centre for Living Systems, Parc Scientifique de Luminy, 13288 Marseille, France
[2]Max Planck Institute of Biochemistry, Am Klopferspitz, Martinsried, 82152 Munich, Germany
[3]School of Life Science and Engineering, Foshan University, Foshan 52800, Guangdong, China
[4]Department of Physiological Chemistry, Biomedical Center, Ludwig Maximilians University of Munich, Großhaderner Strasse, Martinsried, 82152 Munich, Germany
[5]Division of Biological and Biomedical Systems, School of Science and Engineering, University of Missouri-Kansas City, Rockhill Road, Kansas City, MO 64110, USA
[6]These authors contributed equally
[7]X (formerly Twitter): @SchnorrerL
[8]Lead contact
*Correspondence: frank.schnorrer@univ-amu.fr
https://doi.org/10.1016/j.cub.2024.07.079

SUMMARY

Muscle morphogenesis is a multi-step program, starting with myoblast fusion, followed by myotube-tendon attachment and sarcomere assembly, with subsequent sarcomere maturation, mitochondrial amplification, and specialization. The correct chronological order of these steps requires precise control of the transcriptional regulators and their effectors. How this regulation is achieved during muscle development is not well understood. In a genome-wide RNAi screen in *Drosophila*, we identified the BTB-zinc-finger protein Tono (*CG32121*) as a muscle-specific transcriptional regulator. *tono* mutant flight muscles display severe deficits in mitochondria and sarcomere maturation, resulting in uncontrolled contractile forces causing muscle rupture and degeneration during development. Tono protein is expressed during sarcomere maturation and localizes in distinct condensates in flight muscle nuclei. Interestingly, internal pressure exerted by the maturing sarcomeres deforms the muscle nuclei into elongated shapes and changes the Tono condensates, suggesting that Tono senses the mechanical status of the muscle cells. Indeed, external mechanical pressure on the muscles triggers rapid liquid-liquid phase separation of Tono utilizing its BTB domain. Thus, we propose that Tono senses high mechanical pressure to adapt muscle transcription, specifically at the sarcomere maturation stages. Consistently, *tono* mutant muscles display specific defects in a transcriptional switch that represses early muscle differentiation genes and boosts late ones. We hypothesize that a similar mechanoresponsive regulation mechanism may control the activity of related BTB-zinc-finger proteins that, if mutated, can result in uncontrolled force production in human muscle.

INTRODUCTION

Muscle cells, also called muscle fibers, house thousands of contractile machines called sarcomeres. Each sarcomere is a stereotyped unit with a highly ordered architecture in which bipolar myosin filaments face toward highly ordered actin filaments. These actin filaments are cross-linked at the Z-discs bordering each sarcomere. Actin and myosin filaments are stably connected by titin springs.[1–4] Specific muscle fiber types differ in their transcriptional program, resulting in differences in their biomechanical properties.[5–7] As sarcomere architecture is conserved from flies to humans, *Drosophila* is a valid model to study sarcomere morphogenesis.[8,9]

Striated muscle fibers form by a series of developmental events: myoblasts fuse to myotubes,[10] which elongate and attach to tendon cells.[11,12] After attachment, myotubes convert to myofibers by assembling immature myofibrils.[9,13–16] These immature myofibrils consist of chains of immature sarcomeres, which are about 1.2 μm long in young zebrafish muscles[17,18] and 1.8 μm long in early *Drosophila* flight muscles.[15,19] Next, these sarcomeres mature and grow to a length of about 3.4 μm in adult flight muscles.[19,20] During this maturation, each sarcomere incorporates specific sarcomere proteins,[19] resulting in the remarkable regularity of mature sarcomeres. Defects in sarcomere maturation can cause uncontrolled muscle contractions and severe muscle degeneration or atrophy in vertebrates[21–23] and flies.[19,24–27] Hence, correct sarcomere maturation is critical for regulated muscle force production.

In parallel to sarcomere morphogenesis, muscle fibers reorganize various other internal structures. Fibers assemble the

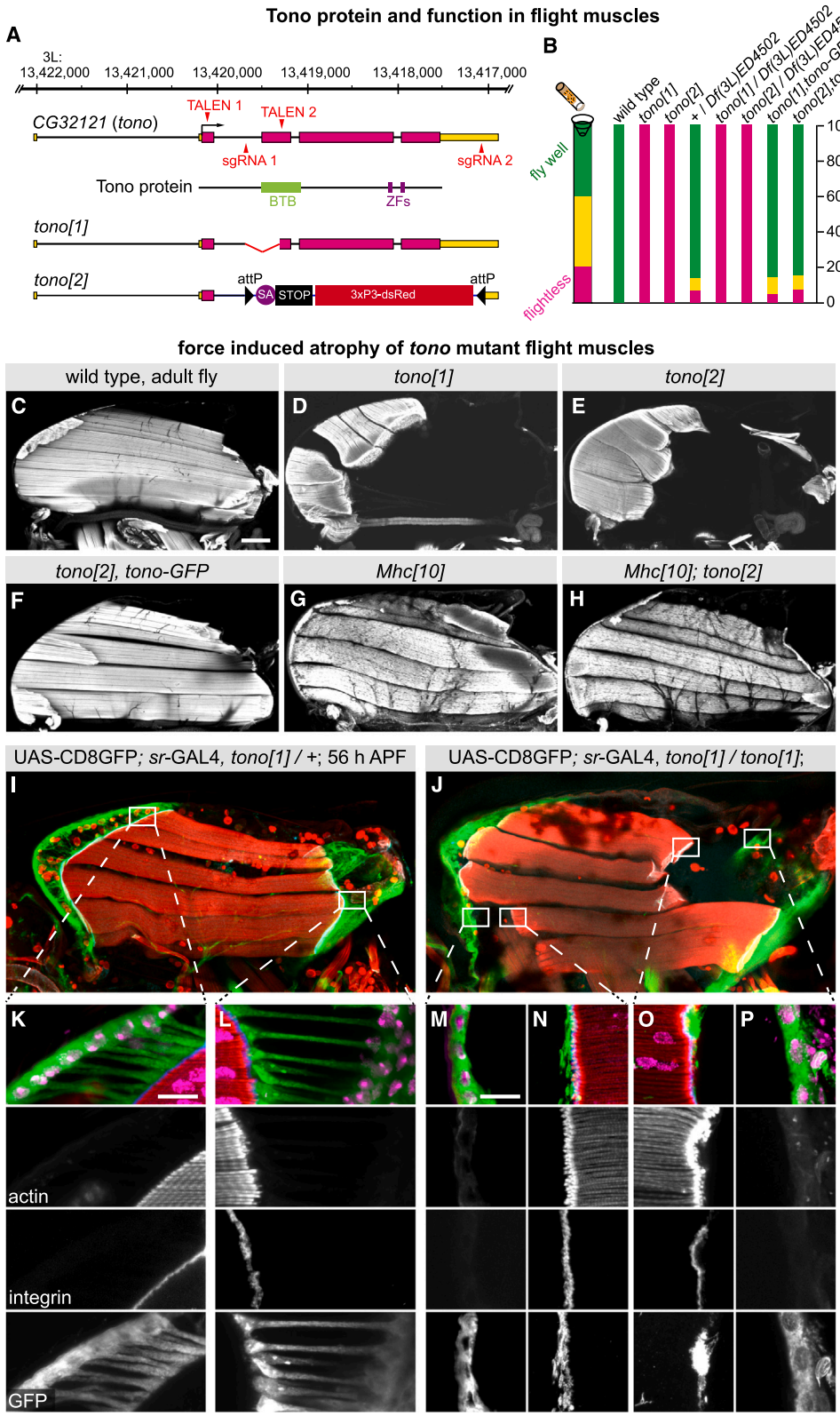

Figure 1. *tono* gene structure and flight muscle phenotypes

(A) Tono gene structure, including the TALEN and sgRNA sites used to generate the *tono[1]* and *tono[2]* alleles.

(B) Flight test of the indicated genotypes.

(legend continued on next page)

postsynaptic part of the neuromuscular junction,[28] position their nuclei equally throughout the fiber,[29,30] and gain a large number of mature mitochondria,[31–34] which match the metabolic needs of each muscle fiber type.[35,36] All these internal structures are densely packed, resulting in high internal pressure in muscles, with the myofibrils pushing the growing mitochondria into elongated shapes.[34] How developing muscles coordinate and accomplish these processes correctly in space and time is not well understood.

Here, we use the *Drosophila* indirect flight muscles to gain insight into how the transcriptional program of developing muscles is dynamically adjusted to match the needs of each stage. We have previously shown that sarcomeres develop in an ordered sequence in flight muscles. Following assembly of immature sarcomeres into myofibrils at 30 h after puparium formation (APF),[15] additional immature sarcomeres are added to the existing myofibrils until 48 h APF, but each sarcomere remains short and thin. After 48 h APF, sarcomeres mature and grow in length and thickness to reach about 3.4 μm.[3,19,20] The sarcomere maturation phase is initiated by a transcriptional switch that downregulates a large number of genes after 30 h APF, whereas other genes are strongly upregulated.[19] This switch needs to be precise, as even reducing levels of single sarcomere proteins can result in dominant flightless phenotypes[37–39] or flight muscle degeneration.[27] Heterozygous loss-of-function mutations in individual sarcomere proteins can also cause dominant cardiomyopathies in humans.[40,41] Thus, the expression levels of the various sarcomere components must be tightly controlled.

Here, we identified a role for *tono* (*CG32121*), a BTB-zinc (Zn)-finger transcriptional regulator, during indirect flight muscle morphogenesis. *tono* mutant flight muscles show a defective transcriptional switch after sarcomere assembly, resulting in severe sarcomere and mitochondria defects. Tono protein is present in muscle nuclei in mechanosensitive condensates, which fuse in response to acute mechanical pressure. Thus, we propose that Tono senses an increase in mechanical pressure during development to adapt the transcriptional status of the muscle to the developmental stage. This transcriptional adaptation contributes to sarcomere and mitochondria maturation.

RESULTS

The BTB-Zn-finger *tono* is required for flight muscle morphogenesis

A genome-wide muscle-specific RNAi screen identified a potential role for *CG32121* during flight muscle development.[42] *CG32121* was recently also found to be expressed in a muscle-specific manner.[43] *CG32121* is located on the third chromosome and encodes a BTB-Zn-finger protein, for which no classical mutants were available (Figure 1A). We used our established TALEN and CRISPR protocols[44,45] to generate two *CG32121* deletion alleles (Figure 1A). We gave *CG32121* the name *tono*, for the phenotypic characteristics described below. The TALEN-induced *tono[1]* allele contains a 363 bp deletion removing the splice acceptor of the second exon and a large part of the BTB domain. In the CRISPR-induced *tono[2]* allele, we exchanged most of the *tono* locus with a STOP cassette (Figure 1A). Both *tono* alleles are homozygous viable but flightless, either homozygous or trans-heterozygous over a large deficiency, showing that *tono* is essential for flight (Figure 1B; see Data S1 for more information).

Histological analysis of the indirect flight muscles in *tono* mutants showed that *tono* is required for flight muscle formation or maintenance, as young mutant adults displayed severe flight muscle degeneration or atrophy (Figures 1C–1E and S1A–S1D). Importantly, this muscle phenotype could be fully rescued by re-expressing Tono-GFP under endogenous control using a GFP-tagged genomic fosmid[46] (Figures 1F, S1E, and S1F), demonstrating that the *tono* loss-of-function phenotype is specific and that the *tono-GFP* fosmid is functional. The *tono* phenotype can also be rescued by re-expressing *tono-HA* in the developing flight muscles (Figures S1H–S1J). Together, these data demonstrate that the BTB-Zn-finger *tono* is required in muscles to prevent flight muscle degeneration.

tono mutant muscles produce abnormally high forces during development

To identify the origin of muscle degeneration in *tono* mutants, we investigated flight muscle development during pupal stages. We found that *tono* mutant flight muscles look normal until 48 h APF and are normally innervated by their motor neurons (Figures S1K–S1Z). However, from 56 h APF onward, *tono[1]* flight muscles progressively detach. Detachment starts primarily at the posterior attachment sites in *tono[1]*, whereas *tono[2]* flight muscles stretch and display severe muscle thinning, eventually resulting in muscle rupture (Figures S1K–S1W).

To closely investigate the detachment phenotype, we labeled the tendon cell membrane. At 56 h APF, the wild-type tendon cells show the force-induced straight extensions from their basal side reaching the muscle fibers (Figures 1I, 1K, and 1L).[15] Surprisingly, in the detached *tono[1]* mutant muscles, tendon cell membranes remained at the detached muscle ends (Figures 1J and 1M–1P). This demonstrates that the tendons themselves (and not the muscle-tendon junction) have been ruptured from the tendon cell body. As this phenotype can be rescued by muscle-specific expression of *tono* (Figures S1H–S1J), these data provide strong evidence that forces produced in *tono[1]* muscles after 48 h APF are too high, resulting in tendon cell rupturing and muscle degeneration. To test this muscle force-induced rupture hypothesis directly, we crossed the *tono* mutants into an *Mhc[10]* background, which lacks force-producing Mhc in flight muscles.[3,47] Indeed, the muscle detachment or rupture phenotypes are entirely rescued in *tono[1]* or *tono[2], Mhc[10]* double

(C–H) Adult hemi-thoraces of wild type (C), *tono[1]* (D), *tono[2]* (E), *tono[2], tono-GFP* fosmid (F), *Mhc[10]* (G), and *Mhc[10]; tono[2]* (H) stained with phalloidin (F-actin).

(I–P) Overview of heterozygous (I) and homozygous *tono[1]* pupae (J) at 56 h APF expressing CD8-GFP in all tendon cells, phalloidin (red), β-integrin (blue), and nuclei (magenta). High magnification of the anterior (K) or posterior tendon (L) of heterozygous or homozygous *tono[1]* (M–P).

Scale bars, 100 μm (C–J) and 10 μm (K–P).

See also Figure S1 and Data S1.

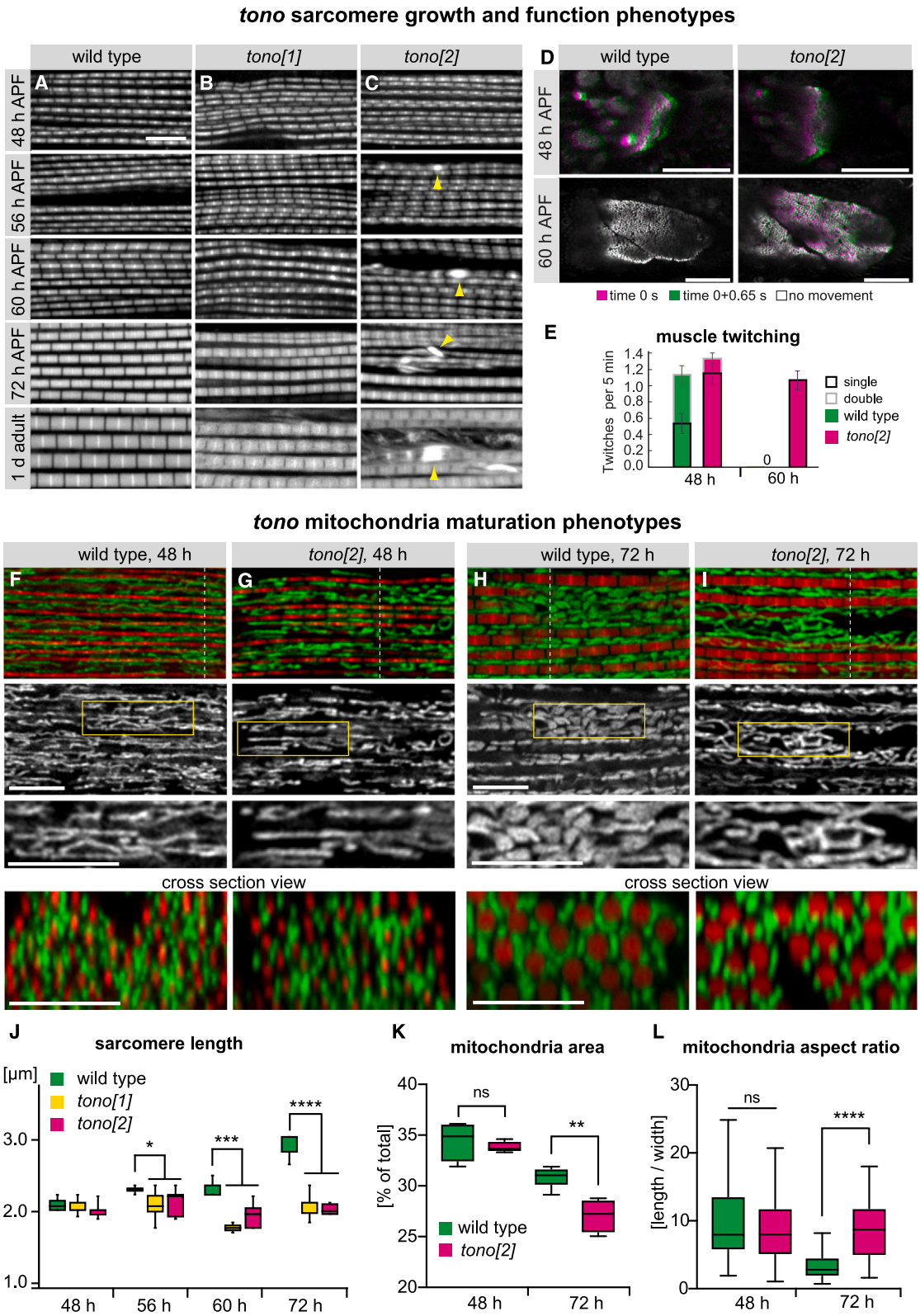

Figure 2. *tono* sarcomere and mitochondria phenotypes

(A–C) Developing myofibrils from wild-type (A), *tono[1]* (B), and *tono[2]* (C) flight muscles stained with phalloidin. Arrowheads indicate large actin accumulations. (D and E) Living wild-type or *tono[2]* flight muscles expressing talin-C-YPet at 48 and 60 h APF (D). Two images from 0 s (magenta) and 0 + 0.65 s (green) were overlayed. White indicates no contraction; green and magenta show contractions. (E) Twitch frequencies of the muscle per 5 min, error bars SEM.

(legend continued on next page)

mutants (Figures 1G, 1H, and S1G), demonstrating that high sarcomere forces in *tono* mutants cause fiber tearing and detachment.

Tono is required for sarcomere and mitochondria maturation

To understand the cause of ectopic force production, we investigated sarcomere and mitochondria morphologies in developing *tono* flight muscles. Until 48 h APF, sarcomere morphology and length are comparable to wild type (Figures 2A–2C and 2J). This shows that sarcomere assembly and addition do not require *tono*. After 48 h APF, wild-type sarcomeres mature and grow from 2 μm to about 2.9 μm in length at 72 h APF. However, *tono* mutant sarcomeres fail to grow and remain about 2 μm long (Figures 2A–2C and 2J). This growth defect is accompanied by actin accumulations in *tono[2]* myofibrils from 56 h APF onward (Figure 2C). These more severe sarcomere integrity phenotypes in *tono[2]* may explain why the *tono[2]* fibers rupture internally while the *tono[1]* muscles shred their tendon cells.

To investigate the functional consequences of this sarcomere maturation defect directly, we assayed the spontaneous twitching of flight muscles in living pupae. As reported before, we found that wild-type flight muscles display spontaneous twitching at 48 h APF, which ceases by 60 h APF when sarcomeres have adapted stretch-activation properties.[19] However, we found robust twitches in *tono* flight muscles at 60 h APF (Figures 2D and 2E; Videos S1 and S2). Together, these data demonstrate a severe sarcomere maturation defect in *tono* mutants that results in ectopic active forces in flight muscles, likely caused by a failure to build stretch-activated sarcomeres.

In concert with the sarcomeres, the mitochondria network undergoes growth to fuel the contractions of mature muscle.[34] By assaying mitochondria morphology, area, and aspect ratio, we found that mitochondria in *tono* mutant flight muscles intercalated normally between the assembled myofibrils and form their normal elongated tube-like morphology at 48 h APF (Figures 2F, 2G, 2K, and 2L). However, while wild-type mitochondria mature to shorter and fatter shapes at 72 h APF, *tono* mutant mitochondria maintain thinner, elongated shapes that are typical for 48 h APF (Figures 2F–2I). Consequently, *tono* mutant mitochondria fail to change their aspect ratio and cover less area, demonstrating their severe maturation defects (Figures 2K and 2L). Together, this demonstrates that *tono* is important for proper flight muscle maturation after 48 h APF.

Tono is expressed in body muscle nuclei

The dramatic defects observed in *tono* mutant flight muscles made us wonder whether Tono protein is indeed a transcriptional regulator, as suggested by its domains. To address this, we first analyzed Tono expression using the functional Tono-GFP fosmid. We found that Tono-GFP is localized within the nuclei of adult body muscles, including indirect flight, jump, and leg muscles. However, Tono-GFP expression is not detectable in visceral muscles, cardiomyocytes, ventral-longitudinal muscles sitting below the adult heart, or other cell types of the adult thorax (Figures 3A–3E), consistent with the fly cell atlas mRNA expression data.[43] This demonstrates that Tono is expressed specifically in a subset of adult striated body muscles.

To test if Tono has a function outside of flight muscles, we performed locomotion and jump assays with adult flies and found that *tono[2]* mutants can walk normally; however, they are severely compromised in their ability to jump (Video S3). This is accompanied by normal sarcomeres in leg muscles but severely shortened and irregular sarcomeres in jump muscles in *tono[2]* (Figures S2A–S2F). Thus, Tono's function appears largely restricted to indirect flight and jump muscles.

As Tono has a role during muscle development, we investigated its mRNA and protein expression dynamics during pupal stages. We found that *tono* mRNA expression is induced at 24 h and peaks at 30 h APF in flight muscles (Figure S2G).[19] Tono-GFP protein is barely detectable at 30 h APF when immature sarcomeres assemble (Figure 3F). At 34 h APF, Tono-GFP is present in indirect flight muscle nuclei, and its expression strongly increases until 48 h, remaining high until 72 h APF (Figures 3G–3J). Thus, the Tono protein is expressed in the flight muscle just before the observed muscle maturation phenotypes are visible in *tono* mutants.

Tono requires its BTB and Zn-finger domains

Next, we wanted to investigate the roles of the BTB and Zn-finger domains. The CRISPR-generated *tono[2]* allele contains two flanking attP sites that can be utilized for phiC31 recombinase-mediated cassette exchange (RMCE) to engineer any designed *tono* allele.[45,48–50] We inserted a *tono* cDNA tagged at the C terminus with 2xHA, which will splice in frame with the remaining 38 amino acids of the endogenous first *tono* exon (*tono-HA*). We also inserted mutant *tono* cDNAs that are either lacking their BTB (*tono-ΔBTB-HA*) or Zn fingers (*tono-ΔZFs-HA*) (Figure 3K). All three hemagglutinin (HA)-tagged proteins are expressed at comparable levels, as assayed by western blot from thorax extracts (Figure S3A), and the flies are homozygous viable. However, only the *tono-HA* flies can fly, whereas *tono-ΔBTB-HA* and *tono-ΔZFs-HA* are flightless (Figure 3L). We analyzed their flight muscle morphology found that *tono-HA* flight muscles are normal and their sarcomeres grow normally. By contrast, both *tono-ΔBTB-HA* and *tono-ΔZFs-HA* alleles display the typical myofiber rupture phenotype of *tono* null alleles at 72 h APF, with severe sarcomere defects (Figures 3M and S3B–S3J). This demonstrates that Tono requires both its BTB and Zn-finger domains to function.

(F–I) Myofibrils (red, phalloidin) and mitochondria (green, mit-GFP) of wild-type (F and H) and *tono[2]* flight muscles (G and I) at 48 and 72 h APF were imaged with a Zeiss airyscan confocal. Yellow boxes show zoom-ins. Cross-sections at the indicated lines are below.
(J–L) Quantification of sarcomere length (J), mitochondria area (K), and mitochondria aspect ratio (L) from the above genotypes. $^{*}p < 0.05$, $^{**}p < 0.01$, $^{***}p < 0.001$, $^{****}p < 0.0001$, two-tailed unpaired Student's t test. Box-and-whisker plots show median as lines, 1st quartile and 2nd quartile as box, and the min-max values in the whiskers.
Scale bars, 5 μm (A–C and F–I) and 50 μm (D).
See also Data S1 and Videos S1 and S2.

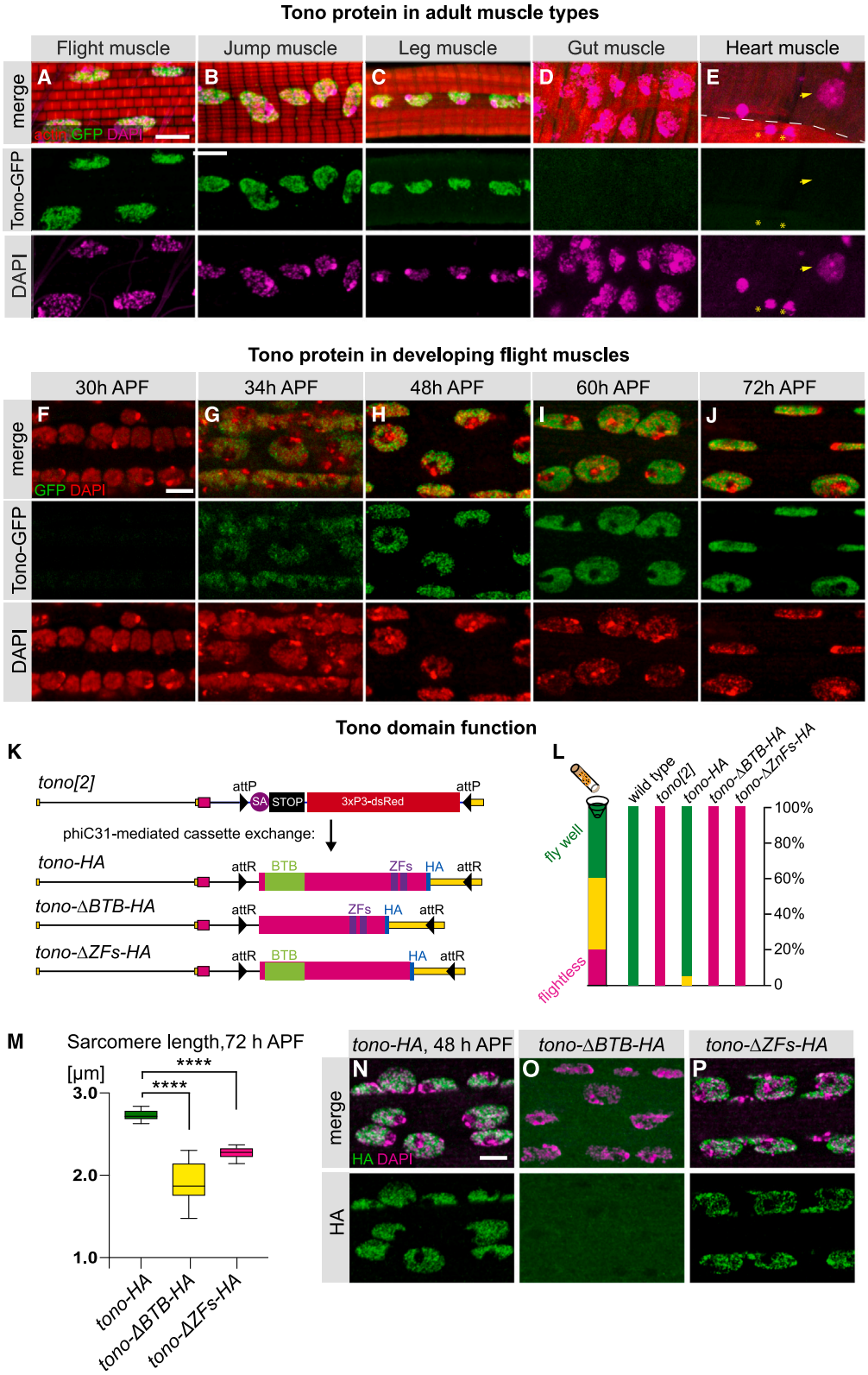

Figure 3. Tono protein expression and localization

(A–E) Expression of Tono-GFP in dorsal-longitudinal flight muscle (A), jump muscle (B), leg muscle (C), visceral muscle (D), and heart (E; yellow arrow marks a cardiomyocyte nucleus, and asterisks mark nuclei of ventral-longitudinal muscles).

(legend continued on next page)

The BTB domain of BTB Zn-finger proteins often mediates protein-protein interactions, whereas Zn fingers are often implicated in binding to DNA.[51] We investigated the distribution of Tono full length and Tono deletions during flight muscle development and found that Tono-ΔBTB-HA is defective in nuclear enrichment, resulting in an equal distribution between cytoplasm and nuclei at 48 h APF (Figures 3N and 3O). By contrast, Tono-ΔZFs-HA is normally localized in the muscle nuclei (Figures 5N and 5P), consistent with the interpretation that Tono's Zn fingers are not required for nuclear localization but rather for its function, possibly for its interaction with DNA. The same Tono localization patterns are present in jump and leg muscles in the *tono* deletion alleles (Figures S3K–S3R).

Tono regulates a metabolic switch during muscle maturation

To test if Tono regulates transcription during muscle development, we dissected indirect flight muscles from wild type and *tono[1]* mutants at 30 and 48 h APF and performed transcriptomics analysis. In accordance with the wild-type morphology and the low expression of Tono at 30 h APF, we found few changes at 30 h APF, but a large number of genes (>2,000 genes) were differentially expressed at 48 h APF in *tono[1]* compared with wild type (Figures S4A and S4B; see Data S2 for more information). This demonstrates that Tono is indeed a transcriptional regulator during muscle maturation stages.

We previously showed that developing wild-type flight muscles undergo a dramatic transcriptional switch between 30 and 48 h APF, with more than 3,000 genes being up- or downregulated,[19] which we reproduced here (Data S2). Comparing wild type to *tono* mRNA-seq data revealed that this transcriptional switch is impaired in *tono* mutant muscles, with many genes being less downregulated or less upregulated than in wild type (Figure 4A). This difference in expression is particularly pronounced for genes that had been previously assigned to developmental clusters that change expression between 30 and 48 h APF in wild type (Figures 4B and S5).[19] This is consistent with Tono being a transcriptional regulator with an important role at this key stage of development.

In accordance with our phenotypic data demonstrating a mitochondrial defect, the developmental clusters 16 and 28 had been shown to be enriched for metabolic pathways, including glycolysis and oxidative phosphorylation (OXPHOS) (Figure 4B).[19] We found similar pathways, including TCA cycle and glycolysis, as being among the top *tono*-regulated KEGG pathways at 48 h APF (48 h *tono[1]* vs. wild type; Data S2). To explore the dynamics of the metabolic pathways in more detail, we used the mitoXplorer tool[53,54] and the Phasik method[52] and applied them to developing flight muscles using our previously published wild-type time course mRNA-seq data.[19] These methods identified a metabolic switch between 30 and 48 h APF, with glycolysis and one carbon metabolism being dominant before 40 h APF and OXPHOS, TCA cycle, and protein synthesis in mitochondria being dominant after 40 h APF (Figure 4C; see Data S3 for more information). This switch is impaired in *tono* mutant muscles. We found that the mitochondrial translation machinery is less upregulated at 48 h APF in *tono* compared with wild type. Consequently, the mitochondria-encoded OXPHOS components, including mt:ND4L and mt:ATPase8, are strongly downregulated, as well as large numbers of the nuclear-encoded OXPHOS components, including ATP synthase β (Figures 4D and S4C). By contrast, phosphofructokinase (Pfk), the rate-limiting enzyme of glycolysis, as well as the pyruvate processing enzyme lactate dehydrogenase (LDH) fail to be downregulated in *tono* (Figures 4D and S4C). We further confirmed the LDH downregulation *in vivo* with an LDH-cherry fusion under endogenous control[55] (Figure 4E). Together, these data demonstrate that Tono transcriptionally instructs the metabolic switch during mid-stages of flight muscle development.

The second large class of genes that change expression during mid-stages of muscle development code for microtubule and actin dynamics, as well as for sarcomere proteins, the latter of which are strongly induced.[19] Again, we find that this switch is impaired in *tono* mutants with the key sarcomere components Mhc, Actn, Zasp52, Zasp66, Unc89/Obscurin, and the titin homologs bt/Projectin and sls being downregulated (Figure 4D; Data S2). We verified the increased expression of the actin-severing protein Gelsolin, which is normally downregulated from 30 to 48 h APF, in *tono* mutants (Figure 4F). We also verified that the expression of the sarcomere Z-disc component Zasp66, whose expression normally increases from 30 to 48 h, is reduced in *tono* mutants (Figure 4G). These transcriptional changes may explain the sarcomere growth defect and the uncontrolled high forces in *tono* mutant muscles by possibly changing the ultrastructure of their sarcomeres.

Tono localizes to nuclear droplets

How does Tono contribute to this transcriptional change at 48 h APF? By inspecting Tono-GFP or Tono-HA nuclear localization in detail, we discovered that Tono localizes non-homogenously throughout the muscle nuclei in a speckled pattern that is reminiscent of phase-separated condensates (Figure 5A). This pattern reminded us of stress granules that were reported *in vitro* to respond to osmotic stress.[56] To test if the Tono localization pattern also responds to osmotic stress, we incubated 48 h APF pupae for 30 min with PBS or PBS plus 250 mM NaCl to mimic osmotic stress. Interestingly, we found that the small Tono-GFP droplets observed in directly fixed or PBS-treated muscle nuclei condense into large droplets after incubation in high salt (Figures 5A–5C), demonstrating that the Tono-positive droplets can dynamically rearrange. These Tono droplets are preferentially located at the nuclear periphery (Figures 5B′ and 5C′) and also form at later developmental stages upon osmotic stress (Figures S6A–S6E). They are not

(F–J) Expression of Tono-GFP in developing flight muscles.
(K–P) Scheme of the RMCE strategy creating the *tono-HA*, *tono-ΔBTB-HA*, and *tono-ΔZFs-HA* alleles (K). Adult flight test (L) and sarcomere length in flight muscles at 72 h APF (M). ****$p < 0.0001$, two-tailed unpaired Student's t test. Error bars represent the ±SD. Localization of Tono-HA (N), Tono-ΔBTB-HA (O), and Tono-ΔZFs-HA (P) in 48 h AFP flight muscles.
All scale bars, 5 μm.
See also Figures S2 and S3, Data S1, and Video S3.

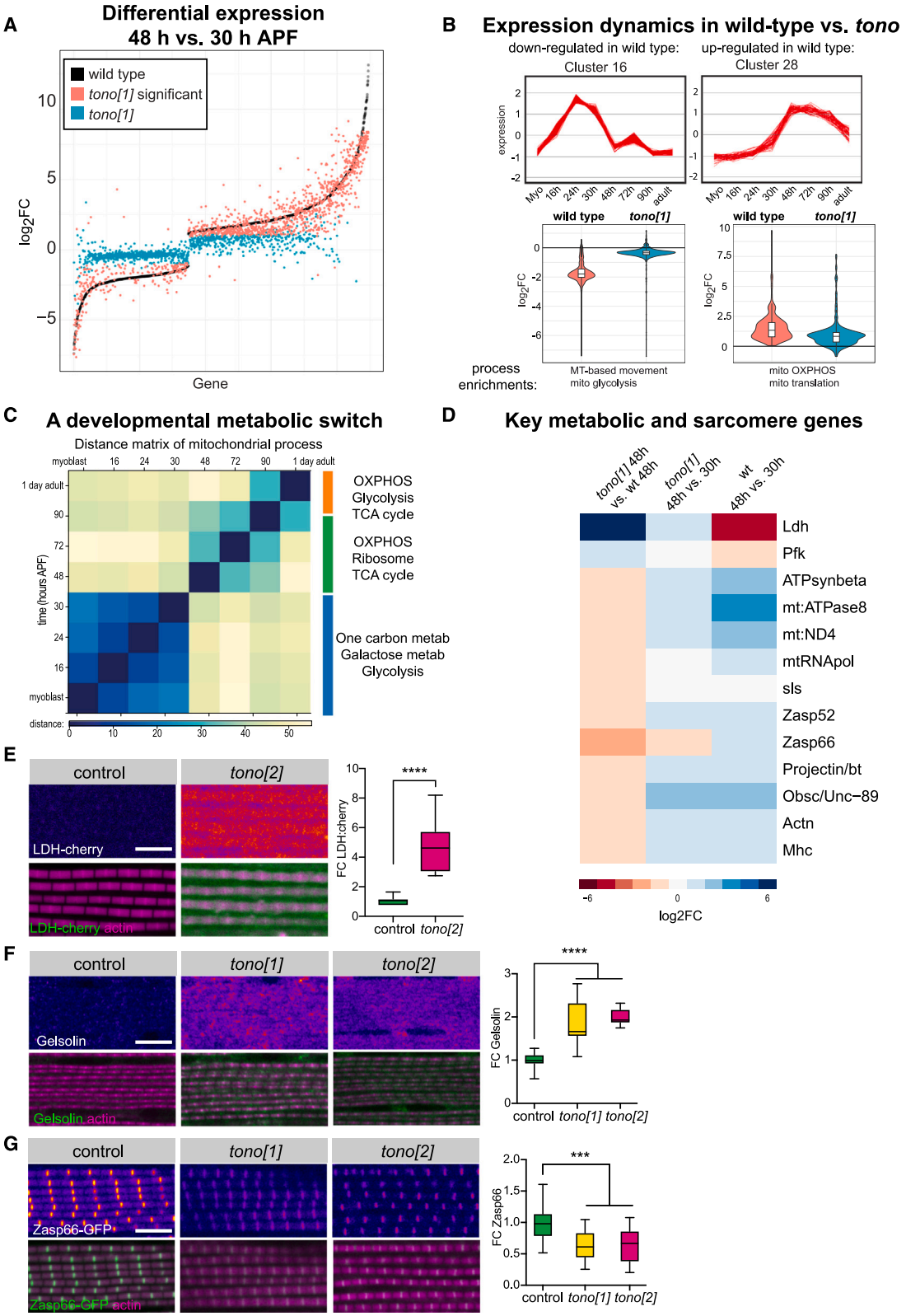

Figure 4. Tono regulates a transcriptional switch

(A) Differential expression of mRNAs from flight muscles comparing 48 to 30 h APF: black lines represent 2,238 significantly changed genes in wild type. The same 2,238 genes are blotted as red or blue dots comparing 48 to 30 h APF in *tono[1]*. Note that most of these genes are above the black line on the left or below the

(legend continued on next page)

enriched for the heterochromatin marker HP1 (Figures S6F and S6G), which forms droplets in early fly embryos or human cells.[57,58] To test which domain of Tono is needed for droplet formation, we tested our HA-tagged Tono deletion mutants and found that the BTB domain but not the Zn fingers is needed for droplet formation (Figures 5D–5I). These findings are in accordance with Tono being a transcriptional regulator whose activity may be adjusted according to the internal status of the muscle cell.

Tono droplets are distinct from insulator bodies

A similar re-localization upon osmotic stress had been described *in vitro* for a class of proteins called insulator bodies, including CP190, BEAF-32, Su(Hw), and Mod(mdg4)67.2.[56] CP190 and Mod(mdg4)67.2 also contain BTB domains. As these components are expressed ubiquitously, we hypothesized that Tono may be a muscle-specific component of the insulator complex. However, we found that although all tested insulator components are recruited to droplets upon osmotic stress in flight muscles, Tono-positive droplets are distinct from CP190, BEAF-32, Su(Hw), or Mod(mdg4)67.2 droplets (Figures 5J–5M and S7A–S7G). These data show that Tono droplets are distinct from insulator bodies.

It is important to note that most of the generally accepted insulator complex components appear dispensable for normal *Drosophila* development. Null or strong hypomorphic alleles for *CTCF*, also a core insulator complex member[59]; *BEAF-32*; or *CP190* are viable[60–63] or only pharate lethal, and their flight muscles do not display gross defects (Figures S7H–S7K). Thus, in contrast to the classical insulator complex components, Tono has an essential role in sarcomere and mitochondria maturation during flight muscle development and may fulfill this role by altering its localization pattern in response to the internal status of the muscle cell.

Tono droplets form reversibly

The rapid formation of the large, round Tono droplets suggested a mechanism of droplet formation by liquid phase condensation. Such condensates form by a regulated liquid-liquid phase separation (LLPS) process, a widely accepted regulatory phenomenon in biology.[64–67] LLPS droplets are characterized by their highly dynamic nature, their ability to fuse, and the reversibility of droplet formation.[63] Our experiments above demonstrated the dynamic nature of Tono droplets to form larger condensates. Next, we tested if releasing the osmotic stress can result in a dynamic disassembly of Tono-positive droplets. Indeed, we found that incubation in a hyperosmotic solution followed by hypo-osmotic conditions results in droplet disassembly (Figures 5N–5P). Thus, Tono-positive droplets can form reversibly.

Tono droplets respond to forces

What could be the endogenous function of the Tono droplets? We hypothesized that our experimentally applied osmotic stress might model a naturally occurring phenomenon during flight muscle development. Just as osmotic stress transports water out of cells and thus intensifies the internal crowding and intracellular pressure, the radial growth of myofibrils and mitochondria generates crowding and thus increases internal pressure in the adult flight muscles.[34] To test if such a high pressure might be present at 48 h APF and possibly sensed by Tono in the nuclei, we quantified nuclear shapes in flight muscles and found that flight muscles have strongly elongated, flat disc-like shaped nuclei that are squeezed between the bundles of growing mitochondria and myofibrils (Figure 6A). Compared with the less squeezed jump muscle nuclei, the flight muscle nuclei are more elongated (Figures 6A, 6B, and 6D), suggesting a particularly high pressure on the flight muscle nuclei. This pressure is largely produced by the assembled myofibrils, as the nuclei of *Mhc[10]* mutants are more round (Figures 6C and 6D).

To test if the small Tono-GFP droplets respond to pressure on the muscle nuclei, we quantified the Tono-GFP granularity by analyzing the Tono-GFP intensity distributions in the different nuclei. The concentration of Tono in large droplets would result in a larger standard deviation of Tono intensities in the nuclei compared with more homogenously distributed small droplets (Figure S8; see STAR Methods for details). Using these criteria, we found that the granularity in wild-type 48 h APF flight muscles is larger than in jump or *Mhc[10]* mutant flight muscles (Figures 6E–6H). As the forces on the nuclei are lower in jump muscles or *Mhc[10]* mutant flight muscles compared with wild-type flight muscles, these results strongly suggest that Tono droplets are mechanosensitive and thus may sense the internal pressure of the developing flight muscles. Hence, we chose the name Tono, inspired by the tonometer used to measure the pressure within the human eye.

If Tono droplets are mechanosensitive *in vivo*, one may predict that they should grow during development, when pressure is built up. To test this, we investigated nuclear shapes and Tono-GFP droplets in developing flight muscles between 36 and 48 h APF. Interestingly, we indeed found that Tono granularity increases from 36 to 48 h APF (Figures 6I–6L), while also nuclei become slightly more elongated (Figures S6H–S6K). However, already at 36 h APF flight muscle nuclei are significantly

black line on the right, indicating defects in downregulation (left) or upregulation (right) in *tono[1]*. Red dots are still significantly different comparing 48 to 30 h APF in *tono[1]*, but blues ones are not. All data are listed in Data S2.

(B) One selected cluster downregulated at 30 h APF (cluster 16) and one upregulated cluster (cluster 28) are shown with the enriched processes from Spletter et al.[19] Violin plots show that the same genes have weaker expression changes between 48 and 30 h APF in *tono[1]* (blue) compared with wild type (red).

(C) Applying Phasik[52] to the flight muscle developmental data[19] revealed three distinct phases during development: phase 1 dominates until 30 h APF, phase 2 from 48 to 90 h APF, and phase 3 after 90 h. The distance between different stages is indicated in a color code (Data S3).

(D) Log_2FC in wild type and *tono[1]* at 48 vs. 30 h APF of key enzymes of glycolysis, lactate metabolism, and OXPHOS from the transcriptomics data.

(E–G) Verification of the expression changes in control vs. *tono[2]* in 72 h APF flight muscles using an LDH-cherry fusion (E) and 48 h APF flight muscles using anti-gelsolin antibody staining (F) or Zasp66-GFP intensity (G). ***$p < 0.001$, ****$p < 0.0001$, two-tailed unpaired Student's t test. Box-and-whisker plots show median as lines, 1st quartile and 2nd quartile as box, and the min-max values in the whiskers.

Scale bars, 5 μm.

See also Figures S4 and S5 and Data S1, S2, and S3.

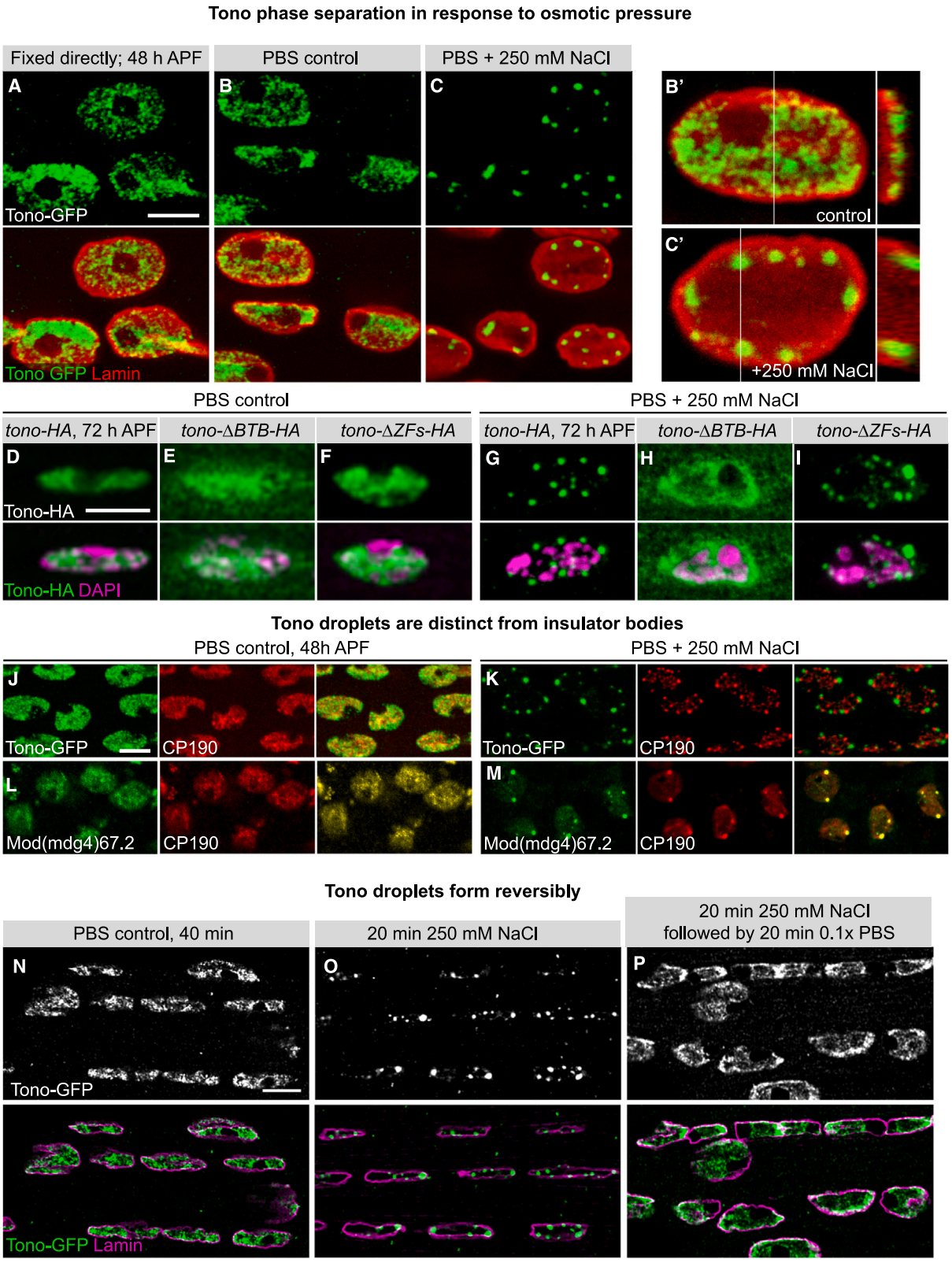

Figure 5. Tono forms droplets in muscle nuclei

(A–C) Tono-GFP localization in flight muscles at 48 h APF fixed directly (A) or incubated with isotonic (B and B′, same nucleus) or hypertonic (C and C′) solution for 30 min. GFP is shown in green and anti-lamin in red.

(legend continued on next page)

elongated, consistent with Tono sensing the pressure status already at this stage of development.

Tono droplets respond to acute force changes

Osmotic pressure is reported to mimic cellular compression forces; however, it is often larger than hydrostatic pressure induced by the cytoskeleton.[68,69] Hence, we wanted to directly increase the mechanical pressure and observe the consequences on Tono droplets. To do so, we mounted living Tono-GFP or CG12356-GFP control flight muscles either "relaxed" with spacers or "squeezed" with the coverslip slightly pressing on the flight muscles. Strikingly, we observed the formation of large Tono-GFP droplets after the squeezed mounting, whereas control CG12356-GFP did not accumulate in droplets (Figures 6M–6P), showing that Tono is selectively sensitive to the mechanical state of the muscle cell. As this mounting method is compatible with live imaging, we discovered that Tono-GFP is highly dynamic and phase-separates into large droplets within a few minutes after the pressure was applied (Figure 6Q; Video S4). This demonstrates that Tono reacts to acute forces on the flight muscle nuclei by forming large droplets.

One important feature of liquid-liquid-phase-separated droplets is their rapid fusion into larger round droplets.[65] By recording high-speed, high-resolution movies of the Tono droplets after mechanical squeezing, we indeed found that smaller Tono droplets fuse to large ones in less than 1 min (Figure 6R; Video S5). Tono-positive droplets therefore meet all three criteria—fusion, dynamic, and reversible—to be classified as LLPS droplets. Together, these results demonstrate that Tono can acutely sense the compression status of flight muscle nuclei and thus may adjust the transcriptional program of the muscle to its developmental status.

DISCUSSION

Muscles are extremely protein-dense tissues that organize their internal organelles and contractile elements with pseudo-crystalline regularity.[70] At the same time, their rigid myofibrils are under high mechanical tension.[15,16,71] This results in a build-up of high internal pressure, with myofibrils squeezing mitochondria and nuclei into elongated shapes.[34,72] However, early during muscle development, protein content and pressure are lower, as myofibrils and mitochondria are thin and nuclei are rounder.[34] Thus, it would be advantageous for a developing muscle fiber to sense when a certain level of pressure has been reached to then trigger the transcriptional program promoting myofibril and mitochondrial growth.[19]

Here, we identified the BTB Zn-finger protein Tono as regulator of this transcriptional switch. In *tono* mutants, the developmental regulation of a group of genes coding for sarcomere and mitochondria components is defective. This results in too short sarcomeres that produce uncontrolled forces, causing muscle tearing and degeneration. Related hypercontraction phenotypes are caused by mutations in the splicing regulator Bruno or the myosin regulators troponin I and troponin T.[24,73–75] However, in these cases, muscle ruptures only occur at the adult stage. Furthermore, *tono* mutant flight muscles display additional defects in their developmental metabolic switch, resulting in a failure of mitochondria growth. This demonstrates the uniqueness of the *tono* phenotype, underscoring its key importance for muscle development.

How does Tono regulate the transcriptional switch? We propose that Tono senses the internal pressure state of the muscle nuclei to instruct transcriptional adaptation, promoting myofibril and mitochondria maturation. The evidence for this hypothesis is fourfold. First, we found that the growing myofibrils and mitochondria squeeze the nuclei into elongated discs at this stage. Second, increasing the internal pressure acutely by hyperosmotic conditions results in a dramatic condensation of Tono protein into large droplets. This treatment induces water efflux from cells and thus dramatically increases the jamming of all components,[76,77] hence likely also the Tono concentration in the nuclei. Formation of these droplets is reversible, demonstrating their dynamic assembly and disassembly. Third, acute mechanical pressure induces the fusion of small Tono droplets into larger ones. This demonstrates the acute mechano-sensitivity of the Tono localization pattern in the nuclei. As the range of mechanically induced hydrostatic pressure is believed to be about 100 times lower than osmotically caused differences,[69,77,78] this result underscores the high mechano-sensitivity of Tono. Fourth and most importantly, the endogenous Tono localization pattern is mechanosensitive as its granularity in the nuclei increases during development when the nuclei elongate, whereas it decreases in response to a reduction of mechanical pressure in myosin mutants. Indeed, transcriptional changes of sarcomere and mitochondria genes have been reported in adult flight muscles of similar *Mhc* mutants as used here.[79] Together, these data strongly suggest that Tono senses mechanical pressure in the flight muscle nuclei during development.

How does Tono droplet formation impact its activity? Tono requires its BTB domain to change its localization in response to pressure. The dynamics of this change follows the typical fast fusion dynamics of smaller droplets to large ones, as described for various LLPSs.[65,67,80] LLPS has been proposed as a mechanism to subdivide the nucleus into different activity domains, with active and inactive DNA compartments, further subdivided into topologically associating domains (TADs)[80,81] and the formation of so-called super-enhancers that result in high expression rates.[82] Established insulator proteins, like CP190 and Mod(mdg4)67.2 also contain BTB Zn-finger domains[81] and

(D–I) Tono-HA (D and G), Tono-ΔBTB-HA (E and H), and Tono-ΔZFs-HA (F and I) in 72 h AFP flight muscles after 30 min incubation in isotonic or hypertonic solution.
(J–M) Co-staining of Tono-GFP (green) with insulator complex components CP190 or Mod(mdg4)67.2 (red) in 48 h AFP flight muscles after 30 min incubation in isotonic (J and L) or hypertonic solution (K and M).
(N–P) Tono-GFP droplets form reversibly. Compare Tono-GFP 40 min in isotonic solution (N) or 20 min in hypertonic solution (O) to 20 min hypertonic solution, followed by 20 min hypotonic solution (P).
All scale bars, 5 μm.
See also Figures S6 and S7 and Data S1.

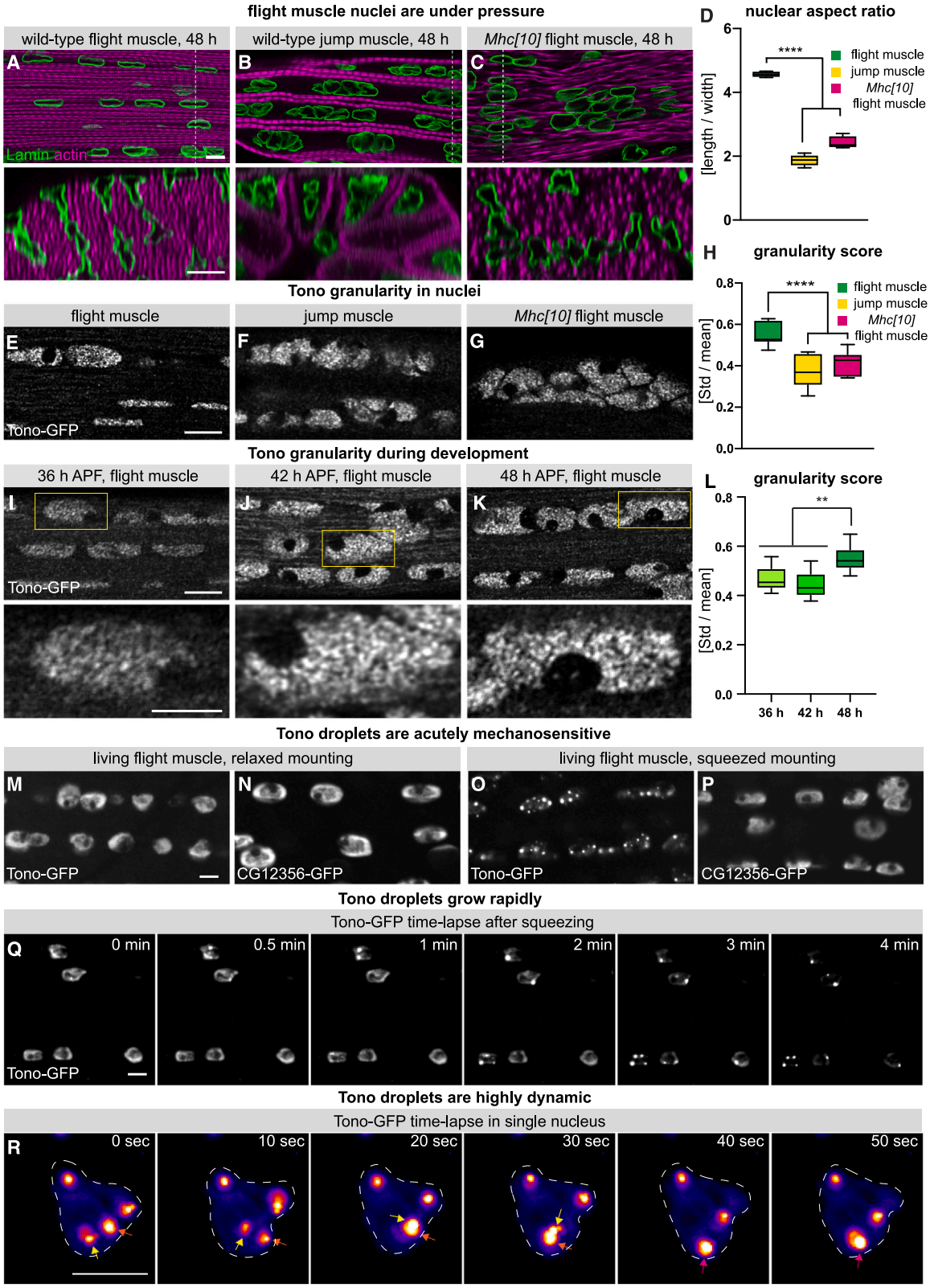

Figure 6. Tono droplets are acutely mechanosensitive

(A–C) 48 h APF wild-type flight muscle (A), jump muscle (B), and *Mhc[10]* mutant flight muscle stained with anti-lamin (nuclei, green) and phalloidin (magenta). Cross-section views at lines are below.

(legend continued on next page)

condense into large droplets distinct from the Tono droplets under high osmotic pressure. What makes Tono special is that the protein is mechanosensitive and that it displays a muscle-specific loss-of-function phenotype. Hence, it is conceivable that Tono does impact chromosome organization or DNA binding in response to mechanical pressure. However, currently, it is unknown if and where the Tono Zn fingers bind to DNA. As chromatin-immunoprecipitation experiments from flight muscles have proven difficult,[36] solving this important question will require additional tools in the future.

The nucleus is a prime organelle where multiple sensory inputs are integrated to monitor the mechanical status of a cell.[83] It can directly sense cellular osmolarity in plant cells and respond to dehydration or mechanical impact by changing transcription.[84] Deformation of the nuclear membrane in mammalian cells can also signal to the actomyosin cytoskeleton via the activation of a cytosolic phospholipase to for example allow rapid squeezing of migratory cells through fine pores.[85,86] Particularly relevant for muscle cells is a MAP3K called ZAKβ that was recently shown to change its activity and localization in the nucleus in response to compression or cyclic contraction in mammalian muscle cells.[68] ZAKβ mutant mice display muscle nuclei position defects and show deficits in sarcomere protein expression and muscle maintenance.[68] Furthermore, mutations in lamins or KASH-SUN proteins in the nuclear membrane that are implicated in mechano-sensing[87,88] cause severe Emery-Dreifuss muscular dystrophies.[89] This underscores the importance of pressure sensing in muscle cells from their birth to their death.

Mammalian genomes contain about 50 BTB Zn-finger genes with no clear Tono homolog. However, mutations in the human BTB Zn-finger ZBTB42 result in lethal congenital contractures at birth. ZBTB42 is highly expressed in muscles, and zebrafish knockdown larvae show severe sarcomere and myofibril defects,[23] suggesting that ZBTB42 might be a functional homolog of Tono in vertebrate muscles.

STAR★METHODS

Detailed methods are provided in the online version of this paper and include the following:

SUPPLEMENTAL INFORMATION

Supplemental information can be found online at https://doi.org/10.1016/j.cub.2024.07.079.

ACKNOWLEDGMENTS

We thank Nuno Luis, Dirk Görlich, and the Schnorrer lab for insightful discussions and input on this manuscript. We thank Johannes Bischof, Dirk Görlich, Robert J Johnston Jr., Mariano Labrador, Maria Leptin, Jordan Raff, and Rainer Renkawitz for generous gifts of antibodies and fly strains. We are grateful to the DSHB for antibodies, the Bloomington Drosophila Stock Center for fly strains (NIH P40OD018537), and Flybase for database organization. We are grateful to Christophe Pitaval for fly embryo injections and fly stock maintenance. We thank Fabio Marchiano for generous help in bioinformatics. We are indebted to the IBDM imaging and fly facilities for help with image acquisition, maintenance of the microscopes, and fly food. This work was supported by the Centre National de la Recherche Scientifique (CNRS, F.S. and B.H.H.); the Max Planck Society (F.S. and B.H.H.); Aix-Marseille University (P.M.); the European Research Council under the European Union's Horizon 2020 Programme (ERC-2019-SyG 856118, F.S.); FP/2007-2013/ERC grant 310939 (F.S.); the excellence initiative Aix-Marseille University A*MIDEX (ANR-11-IDEX-0001-02, F.S.); the French National Research Agency with ANR-ACHN MUSCLE-FORCES (F.S.); MITO-DYNAMICS (ANR-18-CE45-0016-01, F.S. and B.H.H.); the Human Frontier Science Program (HFSP, RGP0052/2018, F.S.); the Bettencourt Foundation (F.S.); the Fondation pour la Recherche Médicale (FDT202106012964, J.A.); the Boehringer Ingelheim Fonds (S.B.L.); the France-BioImaging national research infrastructure (ANR-10-INBS-04-01); France 2030, the French Government program managed by the French National Research Agency (ANR-16-CONV-0001); and Excellence Initiative of Aix-Marseille University - A*MIDEX (Turing Centre for Living Systems).

(D) Quantification of nuclear aspect ratios.
(E–H) 48 h APF wild-type flight muscle (E), jump muscle (F), and *Mhc[10]* mutant flight muscle nuclei expressing Tono-GFP were stained with GFP nanobody, imaged with Zeiss airyscan, and Tono-GFP granularity was quantified (H).
(I–L) Developmental dynamics of Tono-GFP granularity visualized with anti-GFP nanobodies at 36 h (I), 42 h (J), and 48 h APF (K). Lower images show high magnification of yellow boxes (I–K). Note that the granularity score increases at 48 h APF (L).
(M–P) Live imaging of adult flight muscles expressing Tono-GFP or CG12356-GFP mounted relaxed (M and N) or squeezed (O and P).
(Q) Live imaging of Tono-GFP granules after squeezing (Video S4).
(R) High-speed live imaging of one nucleus expressing Tono-GFP after squeezing (Video S5). Note that 2 neighboring granules marked by yellow and orange arrows fuse (red arrow). $^{**}p < 0.01$, $^{****}p < 0.0001$, two-tailed unpaired Student's t test. Box-and-whisker plots show median as lines, 1st quartile and 2nd quartile as box, and the min-max values in the whiskers.
All scale bars, 5 μm.
See also Figures S6 and S8, Data S1, and Videos S4 and S5.

AUTHOR CONTRIBUTIONS

Conceptualization, F.S., X.Z., J.A., and B.H.H.; methodology, X.Z., J.A., M.L.S., S.B.L., and P.M.; software, P.M.; investigation and validation, X.Z., J.A., M.L.S., and S.B.L.; visualization, J.A., X.Z., F.S., P.M., B.H.H., and S.B.L.; funding acquisition, F.S. and B.H.H.; supervision, F.S. and B.H.H.; writing – original draft, F.S., X.Z., and J.A. with input from all authors; writing – review & editing, F.S. and J.A. with input from all authors.

DECLARATION OF INTERESTS

The authors declare no competing interests.

Received: August 17, 2023
Revised: May 26, 2024
Accepted: July 22, 2024
Published: August 19, 2024

REFERENCES

1. Ehler, E., and Gautel, M. (2008). The sarcomere and sarcomerogenesis. Adv. Exp. Med. Biol. *642*, 1–14. https://doi.org/10.1007/978-0-387-84847-1_1.
2. Lange, S., Ehler, E., and Gautel, M. (2006). From A to Z and back? Multicompartment proteins in the sarcomere. Trends Cell Biol. *16*, 11–18. https://doi.org/10.1016/j.tcb.2005.11.007.
3. Loison, O., Weitkunat, M., Kaya-Çopur, A., Nascimento Alves, C., Matzat, T., Spletter, M.L., Luschnig, S., Brasselet, S., Lenne, P.-F., and Schnorrer, F. (2018). Polarization-resolved microscopy reveals a muscle myosin motor-independent mechanism of molecular actin ordering during sarcomere maturation. PLoS Biol. *16*, e2004718. https://doi.org/10.1371/journal.pbio.2004718.
4. Dasbiswas, K., Hu, S., Schnorrer, F., Safran, S.A., and Bershadsky, A.D. (2018). Ordering of myosin II filaments driven by mechanical forces: experiments and theory. Philos. Trans. R. Soc. Lond. B Biol. Sci. *373*, 20170114. https://doi.org/10.1098/rstb.2017.0114.
5. Schiaffino, S., and Reggiani, C. (2011). Fiber types in mammalian skeletal muscles. Physiol. Rev. *91*, 1447–1531. https://doi.org/10.1152/physrev.00031.2010.
6. Spletter, M.L., and Schnorrer, F. (2014). Transcriptional regulation and alternative splicing cooperate in muscle fiber-type specification in flies and mammals. Exp. Cell Res. *321*, 90–98. https://doi.org/10.1016/j.yexcr.2013.10.007.
7. Schönbauer, C., Distler, J., Jährling, N., Radolf, M., Dodt, H.-U., Frasch, M., and Schnorrer, F. (2011). Spalt mediates an evolutionarily conserved switch to fibrillar muscle fate in insects. Nature *479*, 406–409. https://doi.org/10.1038/nature10559.
8. Vigoreaux, J.O. (2006). Molecular basis of muscle structure. In Muscle Development in Drosophila Molecular Biology Intelligence Unit (Springer), pp. 143–156. https://doi.org/10.1007/0-387-32963-3_12.
9. Lemke, S.B., and Schnorrer, F. (2017). Mechanical forces during muscle development. Mech. Dev. *144*, 92–101. https://doi.org/10.1016/j.mod.2016.11.003.
10. Kim, J.H., Jin, P., Duan, R., and Chen, E.H. (2015). Mechanisms of myoblast fusion during muscle development. Curr. Opin. Genet. Dev. *32*, 162–170. https://doi.org/10.1016/j.gde.2015.03.006.
11. Schweitzer, R., Zelzer, E., and Volk, T. (2010). Connecting muscles to tendons: tendons and musculoskeletal development in flies and vertebrates. Development *137*, 2807–2817. https://doi.org/10.1242/dev.047498.
12. Schnorrer, F., and Dickson, B.J. (2004). Muscle building: mechanisms of myotube guidance and attachment site selection. Dev. Cell *7*, 9–20. https://doi.org/10.1016/j.devcel.2004.06.010.
13. Sanger, J.W., Wang, J., Fan, Y., White, J., and Sanger, J.M. (2010). Assembly and dynamics of myofibrils. J. Biomed. Biotechnol. *2010*, 858606.. https://doi.org/10.1155/2010/858606.
14. Sparrow, J.C., and Schöck, F. (2009). The initial steps of myofibril assembly: integrins pave the way. Nat. Rev. Mol. Cell Biol. *10*, 293–298. https://doi.org/10.1038/nrm2634.
15. Weitkunat, M., Kaya-Çopur, A., Grill, S.W., and Schnorrer, F. (2014). Tension and force-resistant attachment are essential for myofibrillogenesis in Drosophila flight muscle. Curr. Biol. *24*, 705–716. https://doi.org/10.1016/j.cub.2014.02.032.
16. Weitkunat, M., Brasse, M., Bausch, A.R., and Schnorrer, F. (2017). Mechanical tension and spontaneous muscle twitching precede the formation of cross-striated muscle *in vivo*. Development *144*, 1261–1272. https://doi.org/10.1242/dev.140723.
17. Sanger, J.W., Wang, J., Fan, Y., White, J., Mi-Mi, L., Dube, D.K., Sanger, J.M., and Pruyne, D. (2017). Assembly and maintenance of myofibrils in striated muscle. In The Actin Cytoskeleton Handbook of Experimental Pharmacology, B.M. Jockusch, ed. (Springer International Publishing), pp. 39–75. https://doi.org/10.1007/164_2016_53.
18. Sanger, J.W., Wang, J., Holloway, B., Du, A., and Sanger, J.M. (2009). Myofibrillogenesis in skeletal muscle cells in zebrafish. Cell Motil. Cytoskeleton *66*, 556–566. https://doi.org/10.1002/cm.20365.
19. Spletter, M.L., Barz, C., Yeroslaviz, A., Zhang, X., Lemke, S.B., Bonnard, A., Brunner, E., Cardone, G., Basler, K., Habermann, B.H., et al. (2018). A transcriptomics resource reveals a transcriptional transition during ordered sarcomere morphogenesis in flight muscle. eLife *7*, e34058. https://doi.org/10.7554/eLife.34058.
20. Orfanos, Z., Leonard, K., Elliott, C., Katzemich, A., Bullard, B., and Sparrow, J. (2015). Sallimus and the dynamics of sarcomere assembly in Drosophila flight muscles. J. Mol. Biol. *427*, 2151–2158. https://doi.org/10.1016/j.jmb.2015.04.003.
21. Johnston, J.J., Kelley, R.I., Crawford, T.O., Morton, D.H., Agarwala, R., Koch, T., Schäffer, A.A., Francomano, C.A., and Biesecker, L.G. (2000). A novel nemaline myopathy in the Amish caused by a mutation in troponin T1. Am. J. Hum. Genet. *67*, 814–821. https://doi.org/10.1086/303089.
22. Robinson, P., Lipscomb, S., Preston, L.C., Altin, E., Watkins, H., Ashley, C.C., and Redwood, C.S. (2007). Mutations in fast skeletal troponin I, troponin T, and β-tropomyosin that cause distal arthrogryposis all increase contractile function. FASEB J. *21*, 896–905. https://doi.org/10.1096/fj.06-6899com.
23. Patel, N., Smith, L.L., Faqeih, E., Mohamed, J., Gupta, V.A., and Alkuraya, F.S. (2014). ZBTB42 mutation defines a novel lethal congenital contracture syndrome (LCCS6). Hum. Mol. Genet. *23*, 6584–6593. https://doi.org/10.1093/hmg/ddu384.
24. Spletter, M.L., Barz, C., Yeroslaviz, A., Schönbauer, C., Ferreira, I.R.S., Sarov, M., Gerlach, D., Stark, A., Habermann, B.H., and Schnorrer, F. (2015). The RNA-binding protein Arrest (Bruno) regulates alternative splicing to enable myofibril maturation in *Drosophila* flight muscle. EMBO Rep. *16*, 178–191. https://doi.org/10.15252/embr.201439791.
25. Nongthomba, U., Cummins, M., Clark, S., Vigoreaux, J.O., and Sparrow, J.C. (2003). Suppression of muscle hypercontraction by mutations in the myosin heavy chain gene of *Drosophila melanogaster*. Genetics *164*, 209–222. https://doi.org/10.1093/genetics/164.1.209.
26. Reedy, M.C., Bullard, B., and Vigoreaux, J.O. (2000). Flightin is essential for thick filament assembly and sarcomere stability in Drosophila flight muscles. J. Cell Biol. *151*, 1483–1500. https://doi.org/10.1083/jcb.151.7.1483.
27. Firdaus, H., Mohan, J., Naz, S., Arathi, P., Ramesh, S.R., and Nongthomba, U. (2015). A *cis*-regulatory mutation in troponin-I of *Drosophila* reveals the importance of proper stoichiometry of structural proteins during muscle assembly. Genetics *200*, 149–165. https://doi.org/10.1534/genetics.115.175604.

28. Burden, S.J., Huijbers, M.G., and Remedio, L. (2018). Fundamental molecules and mechanisms for forming and maintaining neuromuscular synapses. Int. J. Mol. Sci. *19*, 490. https://doi.org/10.3390/ijms19020490.

29. Elhanany-Tamir, H., Yu, Y.V., Shnayder, M., Jain, A., Welte, M., and Volk, T. (2012). Organelle positioning in muscles requires cooperation between two KASH proteins and microtubules. J. Cell Biol. *198*, 833–846. https://doi.org/10.1083/jcb.201204102.

30. Roman, W., and Gomes, E.R. (2018). Nuclear positioning in skeletal muscle. Semin. Cell Dev. Biol. *82*, 51–56. https://doi.org/10.1016/j.semcdb.2017.11.005.

31. Cornelissen, T., Vilain, S., Vints, K., Gounko, N., Verstreken, P., and Vandenberghe, W. (2018). Deficiency of parkin and PINK1 impairs age--dependent mitophagy in Drosophila. eLife *7*, e35878. https://doi.org/10.7554/eLife.35878.

32. Park, J., Lee, S.B., Lee, S., Kim, Y., Song, S., Kim, S., Bae, E., Kim, J., Shong, M., Kim, J.-M., et al. (2006). Mitochondrial dysfunction in Drosophila PINK1 mutants is complemented by parkin. Nature *441*, 1157–1161. https://doi.org/10.1038/nature04788.

33. Sauerwald, J., Backer, W., Matzat, T., Schnorrer, F., and Luschnig, S. (2019). Matrix metalloproteinase 1 modulates invasive behavior of tracheal branches during entry into Drosophila flight muscles. eLife *8*, e48857. https://doi.org/10.7554/eLife.48857.

34. Avellaneda, J., Rodier, C., Daian, F., Brouilly, N., Rival, T., Luis, N.M., and Schnorrer, F. (2021). Myofibril and mitochondria morphogenesis are coordinated by a mechanical feedback mechanism in muscle. Nat. Commun. *12*, 2091. https://doi.org/10.1038/s41467-021-22058-7.

35. Lin, J., Wu, H., Tarr, P.T., Zhang, C.-Y., Wu, Z., Boss, O., Michael, L.F., Puigserver, P., Isotani, E., Olson, E.N., et al. (2002). Transcriptional co-activator PGC-1α drives the formation of slow-twitch muscle fibres. Nature *418*, 797–801. https://doi.org/10.1038/nature00904.

36. Poliacikova, G., Barthez, M., Rival, T., Aouane, A., Luis, N.M., Richard, F., Daian, F., Brouilly, N., Schnorrer, F., Maurel-Zaffran, C., et al. (2023). M1BP is an essential transcriptional activator of oxidative metabolism during Drosophila development. Nat. Commun. *14*, 3187. https://doi.org/10.1038/s41467-023-38986-5.

37. Bernstein, S.I., Mogami, K., Donady, J.J., and Emerson, C.P. (1983). Drosophila muscle myosin heavy chain encoded by a single gene in a cluster of muscle mutations. Nature *302*, 393–397. https://doi.org/10.1038/302393a0.

38. Beall, C.J., Sepanski, M.A., and Fyrberg, E.A. (1989). Genetic dissection of Drosophila myofibril formation: effects of actin and myosin heavy chain null alleles. Genes Dev. *3*, 131–140. https://doi.org/10.1101/gad.3.2.131.

39. Cripps, R.M., Ball, E., Stark, M., Lawn, A., and Sparrow, J.C. (1994). Recovery of dominant, autosomal flightless mutants of Drosophila melanogaster and identification of a new gene required for normal muscle structure and function. Genetics *137*, 151–164. https://doi.org/10.1093/genetics/137.1.151.

40. Van Dijk, S.J., Dooijes, D., Dos Remedios, C., Michels, M., Lamers, J.M.J., Winegrad, S., Schlossarek, S., Carrier, L., Ten Cate, F.J., Stienen, G.J.M., et al. (2009). Cardiac myosin-binding protein C mutations and hypertrophic cardiomyopathy: haploinsufficiency, deranged phosphorylation, and cardiomyocyte dysfunction. Circulation *119*, 1473–1483. https://doi.org/10.1161/CIRCULATIONAHA.108.838672.

41. Marston, S., Copeland, O., Jacques, A., Livesey, K., Tsang, V., McKenna, W.J., Jalilzadeh, S., Carballo, S., Redwood, C., and Watkins, H. (2009). Evidence from human myectomy samples that MYBPC3 mutations cause hypertrophic cardiomyopathy through haploinsufficiency. Circ. Res. *105*, 219–222. https://doi.org/10.1161/CIRCRESAHA.109.202440.

42. Schnorrer, F., Schönbauer, C., Langer, C.C.H., Dietzl, G., Novatchkova, M., Schernhuber, K., Fellner, M., Azaryan, A., Radolf, M., Stark, A., et al. (2010). Systematic genetic analysis of muscle morphogenesis and function in Drosophila. Nature *464*, 287–291. https://doi.org/10.1038/nature08799.

43. Li, H., Janssens, J., De Waegeneer, M., Kolluru, S.S., Davie, K., Gardeux, V., Saelens, W., David, F.P.A., Brbić, M., Spanier, K., et al. (2022). Fly Cell Atlas: A single-nucleus transcriptomic atlas of the adult fruit fly. Science *375*, eabk2432. https://doi.org/10.1126/science.abk2432.

44. Zhang, X., Ferreira, I.R.S., and Schnorrer, F. (2014). A simple TALEN-based protocol for efficient genome-editing in Drosophila. Methods *69*, 32–37. https://doi.org/10.1016/j.ymeth.2014.03.020.

45. Zhang, X., Koolhaas, W.H., and Schnorrer, F. (2014). A versatile two-step CRISPR- and RMCE-based strategy for efficient genome engineering in Drosophila. G3 (Bethesda) *4*, 2409–2418. https://doi.org/10.1534/g3.114.013979.

46. Sarov, M., Barz, C., Jambor, H., Hein, M.Y., Schmied, C., Suchold, D., Stender, B., Janosch, S., K J, V.V., Krishnan, R.T., et al. (2016). A genome-wide resource for the analysis of protein localisation in Drosophila. eLife *5*, e12068. https://doi.org/10.7554/eLife.12068.

47. Cripps, R.M., Suggs, J.A., and Bernstein, S.I. (1999). Assembly of thick filaments and myofibrils occurs in the absence of the myosin head. EMBO J. *18*, 1793–1804. https://doi.org/10.1093/emboj/18.7.1793.

48. Venken, K.J.T., Schulze, K.L., Haelterman, N.A., Pan, H., He, Y., Evans-Holm, M., Carlson, J.W., Levis, R.W., Spradling, A.C., Hoskins, R.A., et al. (2011). MiMIC: a highly versatile transposon insertion resource for engineering Drosophila melanogaster genes. Nat. Methods *8*, 737–743. https://doi.org/10.1038/nmeth.1662.

49. Kanca, O., Bellen, H.J., and Schnorrer, F. (2017). Gene tagging strategies to assess protein expression, localization, and function in Drosophila. Genetics *207*, 389–412.

50. Avellaneda, J., and Schnorrer, F. (2022). Tagging Drosophila proteins with genetically encoded fluorophores. In Drosophila Methods in Molecular Biology, C. Dahmann, ed. (Springer), pp. 251–268. https://doi.org/10.1007/978-1-0716-2541-5_12.

51. Siggs, O.M., and Beutler, B. (2012). The BTB-ZF transcription factors. Cell Cycle *11*, 3358–3369. https://doi.org/10.4161/cc.21277.

52. Lucas, M., Morris, A., Townsend-Teague, A., Tichit, L., Habermann, B., and Barrat, A. (2023). Inferring cell cycle phases from a partially temporal network of protein interactions. Cell Rep. Methods *3*, 100397. https://doi.org/10.1016/j.crmeth.2023.100397.

53. Marchiano, F., Haering, M., and Habermann, B.H. (2022). The mitoXplorer 2.0 update: integrating and interpreting mitochondrial expression dynamics within a cellular context. Nucleic Acids Res. *50*, W490–W499. https://doi.org/10.1093/nar/gkac306.

54. Yim, A., Koti, P., Bonnard, A., Marchiano, F., Dürrbaum, M., Garcia-Perez, C., Villaveces, J., Gamal, S., Cardone, G., Perocchi, F., et al. (2020). mitoXplorer, a visual data mining platform to systematically analyze and visualize mitochondrial expression dynamics and mutations. Nucleic Acids Res. *48*, 605–632. https://doi.org/10.1093/nar/gkz1128.

55. Krejčová, G., Danielová, A., Nedbalová, P., Kazek, M., Strych, L., Chawla, G., Tennessen, J.M., Lieskovská, J., Jindra, M., Doležal, T., et al. (2019). Drosophila macrophages switch to aerobic glycolysis to mount effective antibacterial defense. eLife *8*, e50414. https://doi.org/10.7554/eLife.50414.

56. Schoborg, T., Rickels, R., Barrios, J., and Labrador, M. (2013). Chromatin insulator bodies are nuclear structures that form in response to osmotic stress and cell death. J. Cell Biol. *202*, 261–276. https://doi.org/10.1083/jcb.201304181.

57. Strom, A.R., Emelyanov, A.V., Mir, M., Fyodorov, D.V., Darzacq, X., and Karpen, G.H. (2017). Phase separation drives heterochromatin domain formation. Nature *547*, 241–245. https://doi.org/10.1038/nature22989.

58. Larson, A.G., Elnatan, D., Keenen, M.M., Trnka, M.J., Johnston, J.B., Burlingame, A.L., Agard, D.A., Redding, S., and Narlikar, G.J. (2017). Liquid droplet formation by HP1α suggests a role for phase separation in heterochromatin. Nature *547*, 236–240. https://doi.org/10.1038/nature22822.

59. Mohan, M., Bartkuhn, M., Herold, M., Philippen, A., Heinl, N., Bardenhagen, I., Leers, J., White, R.A.H., Renkawitz-Pohl, R., Saumweber, H., et al. (2007). The Drosophila insulator proteins CTCF

and CP190 link enhancer blocking to body patterning. EMBO J. *26*, 4203–4214. https://doi.org/10.1038/sj.emboj.7601851.

60. Cavalheiro, G.R., Girardot, C., Viales, R.R., Pollex, T., Cao, T.B.N., Lacour, P., Feng, S., Rabinowitz, A., and Furlong, E.E.M. (2023). CTCF, BEAF-32, and CP190 are not required for the establishment of TADs in early *Drosophila* embryos but have locus-specific roles. Sci. Adv. *9*, eade1085. https://doi.org/10.1126/sciadv.ade1085.
61. Gambetta, M.C., and Furlong, E.E.M. (2018). The insulator protein CTCF is required for correct Hox gene expression, but not for embryonic development in *Drosophila*. Genetics *210*, 129–136. https://doi.org/10.1534/genetics.118.301350.
62. Kaushal, A., Mohana, G., Dorier, J., Özdemir, I., Omer, A., Cousin, P., Semenova, A., Taschner, M., Dergai, O., Marzetta, F., et al. (2021). CTCF loss has limited effects on global genome architecture in Drosophila despite critical regulatory functions. Nat. Commun. *12*, 1011. https://doi.org/10.1038/s41467-021-21366-2.
63. Kyrchanova, O., Klimenko, N., Postika, N., Bonchuk, A., Zolotarev, N., Maksimenko, O., and Georgiev, P. (2021). Drosophila architectural protein CTCF is not essential for fly survival and is able to function independently of CP190. Biochim. Biophys. Acta Gene Regul. Mech. *1864*, 194733. https://doi.org/10.1016/j.bbagrm.2021.194733.
64. Frey, S., Richter, R.P., and Görlich, D. (2006). FG-rich repeats of nuclear pore proteins form a three-dimensional meshwork with hydrogel-like properties. Science *314*, 815–817. https://doi.org/10.1126/science.1132516.
65. Shin, Y., and Brangwynne, C.P. (2017). Liquid phase condensation in cell physiology and disease. Science *357*, eaaf4382. https://doi.org/10.1126/science.aaf4382.
66. Hyman, A.A., Weber, C.A., and Jülicher, F. (2014). Liquid-liquid phase separation in biology. Annu. Rev. Cell Dev. Biol. *30*, 39–58. https://doi.org/10.1146/annurev-cellbio-100913-013325.
67. Alberti, S., and Hyman, A.A. (2021). Biomolecular condensates at the nexus of cellular stress, protein aggregation disease and ageing. Nat. Rev. Mol. Cell Biol. *22*, 196–213. https://doi.org/10.1038/s41580-020-00326-6.
68. Nordgaard, C., Vind, A.C., Stonadge, A., Kjøbsted, R., Snieckute, G., Antas, P., Blasius, M., Reinert, M.S., Del Val, A.M., Bekker-Jensen, D.B., et al. (2022). ZAKβ is activated by cellular compression and mediates contraction-induced MAP kinase signaling in skeletal muscle. EMBO J. *41*, e111650. https://doi.org/10.15252/embj.2022111650.
69. Venkova, L., Vishen, A.S., Lembo, S., Srivastava, N., Duchamp, B., Ruppel, A., Williart, A., Vassilopoulos, S., Deslys, A., Garcia Arcos, J.M., et al. (2022). A mechano-osmotic feedback couples cell volume to the rate of cell deformation. eLife *11*, e72381. https://doi.org/10.7554/eLife.72381.
70. Luis, N.M., and Schnorrer, F. (2021). Mechanobiology of muscle and myofibril morphogenesis. Cells Dev. *168*, 203760. https://doi.org/10.1016/j.cdev.2021.203760.
71. Swist, S., Unger, A., Li, Y., Vöge, A., Von Frieling-Salewsky, M., Skärlén, Å., Cacciani, N., Braun, T., Larsson, L., and Linke, W.A. (2020). Maintenance of sarcomeric integrity in adult muscle cells crucially depends on Z-disc anchored titin. Nat. Commun. *11*, 4479. https://doi.org/10.1038/s41467-020-18131-2.
72. Roman, W., Martins, J.P., Carvalho, F.A., Voituriez, R., Abella, J.V.G., Santos, N.C., Cadot, B., Way, M., and Gomes, E.R. (2017). Myofibril contraction and crosslinking drive nuclear movement to the periphery of skeletal muscle. Nat. Cell Biol. *19*, 1189–1201. https://doi.org/10.1038/ncb3605.
73. Barbas, J.A., Galceran, J., Torroja, L., Prado, A., and Ferrús, A. (1993). Abnormal muscle development in the heldup3 mutant of Drosophila melanogaster is caused by a splicing defect affecting selected troponin I isoforms. Mol. Cell. Biol. *13*, 1433–1439. https://doi.org/10.1128/mcb.13.3.1433-1439.1993.
74. Nongthomba, U., Ansari, M., Thimmaiya, D., Stark, M., and Sparrow, J. (2007). Aberrant splicing of an alternative exon in the Drosophila troponin-T gene affects flight muscle development. Genetics *177*, 295–306. https://doi.org/10.1534/genetics.106.056812.
75. Nongthomba, U., Clark, S., Cummins, M., Ansari, M., Stark, M., and Sparrow, J.C. (2004). Troponin I is required for myofibrillogenesis and sarcomere formation in *Drosophila* flight muscle. J. Cell Sci. *117*, 1795–1805. https://doi.org/10.1242/jcs.01024.
76. Fischbarg, J. (2010). Fluid transport across leaky epithelia: central role of the tight junction and supporting role of aquaporins. Physiol. Rev. *90*, 1271–1290. https://doi.org/10.1152/physrev.00025.2009.
77. Torres-Sánchez, A., Kerr Winter, M., and Salbreux, G. (2021). Tissue hydraulics: physics of lumen formation and interaction. Cells Dev. *168*, 203724. https://doi.org/10.1016/j.cdev.2021.203724.
78. Mosaliganti, K.R., Swinburne, I.A., Chan, C.U., Obholzer, N.D., Green, A.A., Tanksale, S., Mahadevan, L., and Megason, S.G. (2019). Size control of the inner ear via hydraulic feedback. eLife *8*, e39596. https://doi.org/10.7554/eLife.39596.
79. Madan, A., Thimmaiya, D., Franco-Cea, A., Aiyaz, M., Kumar, P., Sparrow, J.C., and Nongthomba, U. (2017). Transcriptome analysis of IFM-specific actin and myosin nulls in Drosophila melanogaster unravels lesion-specific expression blueprints across muscle mutations. Gene *631*, 16–28. https://doi.org/10.1016/j.gene.2017.07.061.
80. Lafontaine, D.L.J., Riback, J.A., Bascetin, R., and Brangwynne, C.P. (2021). The nucleolus as a multiphase liquid condensate. Nat. Rev. Mol. Cell Biol. *22*, 165–182. https://doi.org/10.1038/s41580-020-0272-6.
81. Amankwaa, B., Schoborg, T., and Labrador, M. (2022). *Drosophila* insulator proteins exhibit in vivo liquid–liquid phase separation properties. Life Sci. Alliance *5*, e202201536. https://doi.org/10.26508/lsa.202201536.
82. Hnisz, D., Shrinivas, K., Young, R.A., Chakraborty, A.K., and Sharp, P.A. (2017). A phase separation model for transcriptional control. Cell *169*, 13–23. https://doi.org/10.1016/j.cell.2017.02.007.
83. Dupont, S., and Wickström, S.A. (2022). Mechanical regulation of chromatin and transcription. Nat. Rev. Genet. *23*, 624–643. https://doi.org/10.1038/s41576-022-00493-6.
84. Goswami, R., Asnacios, A., Milani, P., Graindorge, S., Houlné, G., Mutterer, J., Hamant, O., and Chabouté, M.-E. (2020). Mechanical shielding in plant nuclei. Curr. Biol. *30*, 2013–2025.e3. https://doi.org/10.1016/j.cub.2020.03.059.
85. Venturini, V., Pezzano, F., Català Castro, F., Häkkinen, H.-M., Jiménez-Delgado, S., Colomer-Rosell, M., Marro, M., Tolosa-Ramon, Q., Paz-López, S., Valverde, M.A., et al. (2020). The nucleus measures shape changes for cellular proprioception to control dynamic cell behavior. Science *370*, eaba2644. https://doi.org/10.1126/science.aba2644.
86. Lomakin, A.J., Cattin, C.J., Cuvelier, D., Alraies, Z., Molina, M., Nader, G.P.F., Srivastava, N., Sáez, P.J., Garcia-Arcos, J.M., Zhitnyak, I.Y., et al. (2020). The nucleus acts as a ruler tailoring cell responses to spatial constraints. Science *370*, eaba2894. https://doi.org/10.1126/science.aba2894.
87. Swift, J., Ivanovska, I.L., Buxboim, A., Harada, T., Dingal, P.C.D.P., Pinter, J., Pajerowski, J.D., Spinler, K.R., Shin, J.-W., Tewari, M., et al. (2013). Nuclear lamin-A scales with tissue stiffness and enhances matrix-directed differentiation. Science *341*, 1240104. https://doi.org/10.1126/science.1240104.
88. Wang, S., Stoops, E., Cp, U., Markus, B., Reuveny, A., Ordan, E., and Volk, T. (2018). Mechanotransduction via the LINC complex regulates DNA replication in myonuclei. J. Cell Biol. *217*, 2005–2018. https://doi.org/10.1083/jcb.201708137.
89. Heller, S.A., Shih, R., Kalra, R., and Kang, P.B. (2020). Emery-Dreifuss muscular dystrophy. Muscle Nerve *61*, 436–448. https://doi.org/10.1002/mus.26782.
90. James, T.C., and Elgin, S.C.R. (1986). Identification of a nonhistone chromosomal protein associated with heterochromatin in *Drosophila melanogaster* and its gene. Mol. Cell. Biol. *6*, 3862–3872. https://doi.org/10.1128/mcb.6.11.3862-3872.1986.

91. Collier, V.L., Kronert, W.A., O'Donnell, P.T., Edwards, K.A., and Bernstein, S.I. (1990). Alternative myosin hinge regions are utilized in a tissue-specific fashion that correlates with muscle contraction speed. Genes Dev. *4*, 885–895. https://doi.org/10.1101/gad.4.6.885.

92. Roy, S., Gilbert, M.K., and Hart, C.M. (2007). Characterization of *BEAF* mutations isolated by homologous recombination in Drosophila. Genetics *176*, 801–813. https://doi.org/10.1534/genetics.106.068056.

93. Lemke, S.B., Weidemann, T., Cost, A.-L., Grashoff, C., and Schnorrer, F. (2019). A small proportion of Talin molecules transmit forces at developing muscle attachments in vivo. PLoS Biol. *17*, e3000057. https://doi.org/10.1371/journal.pbio.3000057.

94. Moreno-Mateos, M.A., Vejnar, C.E., Beaudoin, J.-D., Fernandez, J.P., Mis, E.K., Khokha, M.K., and Giraldez, A.J. (2015). CRISPRscan: designing highly efficient sgRNAs for CRISPR-Cas9 targeting in vivo. Nat. Methods *12*, 982–988. https://doi.org/10.1038/nmeth.3543.

95. Dobin, A., Davis, C.A., Schlesinger, F., Drenkow, J., Zaleski, C., Jha, S., Batut, P., Chaisson, M., and Gingeras, T.R. (2013). STAR: ultrafast universal RNA-seq aligner. Bioinformatics *29*, 15–21. https://doi.org/10.1093/bioinformatics/bts635.

96. Haering, M., and Habermann, B.H. (2021). RNfuzzyApp: an R shiny RNA-seq data analysis app for visualisation, differential expression analysis, time-series clustering and enrichment analysis. F1000Res *10*, 654. https://doi.org/10.12688/f1000research.54533.1.

97. Love, M.I., Huber, W., and Anders, S. (2014). Moderated estimation of fold change and dispersion for RNA-seq data with DESeq2. Genome Biol. *15*, 550. https://doi.org/10.1186/s13059-014-0550-8.

98. Kuleshov, M.V., Diaz, J.E.L., Flamholz, Z.N., Keenan, A.B., Lachmann, A., Wojciechowicz, M.L., Cagan, R.L., and Ma'ayan, A. (2019). modEnrichr: a suite of gene set enrichment analysis tools for model organisms. Nucleic Acids Res. *47*, W183–W190. https://doi.org/10.1093/nar/gkz347.

99. Schindelin, J., Arganda-Carreras, I., Frise, E., Kaynig, V., Longair, M., Pietzsch, T., Preibisch, S., Rueden, C., Saalfeld, S., Schmid, B., et al. (2012). Fiji: an open-source platform for biological-image analysis. Nat. Methods *9*, 676–682. https://doi.org/10.1038/nmeth.2019.

100. Bischof, J., Björklund, M., Furger, E., Schertel, C., Taipale, J., and Basler, K. (2013). A versatile platform for creating a comprehensive UAS-ORFeome library in *Drosophila*. Development *140*, 2434–2442. https://doi.org/10.1242/dev.088757.

101. Bryantsev, A.L., Baker, P.W., Lovato, T.L., Jaramillo, M.S., and Cripps, R.M. (2012). Differential requirements for myocyte enhancer factor-2 during adult myogenesis in Drosophila. Dev. Biol. *361*, 191–207. https://doi.org/10.1016/j.ydbio.2011.09.031.

102. Fernandes, J.J., Celniker, S.E., and VijayRaghavan, K. (1996). Development of the indirect flight muscle attachment sites in Drosophila: role of the PS integrins and the stripe gene. Dev. Biol. *176*, 166–184. https://doi.org/10.1006/dbio.1996.0125.

103. Butcher, R.D.J., Chodagam, S., Basto, R., Wakefield, J.G., Henderson, D.S., Raff, J.W., and Whitfield, W.G.F. (2004). The *Drosophila* centrosome-associated protein CP190 is essential for viability but not for cell division. J. Cell Sci. *117*, 1191–1199. https://doi.org/10.1242/jcs.00979.

104. Cermak, T., Doyle, E.L., Christian, M., Wang, L., Zhang, Y., Schmidt, C., Baller, J.A., Somia, N.V., Bogdanove, A.J., and Voytas, D.F. (2011). Efficient design and assembly of custom TALEN and other TAL effector-based constructs for DNA targeting. Nucleic Acids Res. *39*, e82. https://doi.org/10.1093/nar/gkr218.

105. Liao, Y., Smyth, G.K., and Shi, W. (2014). featureCounts: an efficient general purpose program for assigning sequence reads to genomic features. Bioinformatics *30*, 923–930. https://doi.org/10.1093/bioinformatics/btt656.

106. Sun, J., Nishiyama, T., Shimizu, K., and Kadota, K. (2013). TCC: an R package for comparing tag count data with robust normalization strategies. BMC Bioinformatics *14*, 219. https://doi.org/10.1186/1471-2105-14-219.

107. Weitkunat, M., and Schnorrer, F. (2014). A guide to study Drosophila muscle biology. Methods *68*, 2–14. https://doi.org/10.1016/j.ymeth.2014.02.037.

108. Blanton, J., Gaszner, M., and Schedl, P. (2003). Protein:protein interactions and the pairing of boundary elements in vivo. Genes Dev. *17*, 664–675. https://doi.org/10.1101/gad.1052003.

109. Brower, D.L., Wilcox, M., Piovant, M., Smith, R.J., and Reger, L.A. (1984). Related cell-surface antigens expressed with positional specificity in Drosophila imaginal discs. Proc. Natl. Acad. Sci. USA *81*, 7485–7489. https://doi.org/10.1073/pnas.81.23.7485.

110. Zipursky, S.L., Venkatesh, T.R., Teplow, D.B., and Benzer, S. (1984). Neuronal development in the Drosophila retina: molecular antibodies as molecular probes. Cell *36*, 15–26. https://doi.org/10.1016/0092-8674(84)90069-2.

111. Riemer, D., Stuurman, N., Berrios, M., Hunter, C., Fisher, P.A., and Weber, K. (1995). Expression of *Drosophila* lamin C is developmentally regulated: analogies with vertebrate A-type lamins. J. Cell Sci. *108*, 3189–3198. https://doi.org/10.1242/jcs.108.10.3189.

112. Stella, M.C., Schauerte, H., Straub, K.L., and Leptin, M. (1994). Identification of secreted and cytosolic gelsolin in Drosophila. J. Cell Biol. *125*, 607–616. https://doi.org/10.1083/jcb.125.3.607.

113. Lemke, S.B., and Schnorrer, F. (2018). In vivo imaging of muscle-tendon morphogenesis in Drosophila pupae. J. Vis. Exp. 57312. https://doi.org/10.3791/57312.

STAR★METHODS

KEY RESOURCES TABLE

REAGENT or RESOURCE	SOURCE	IDENTIFIER
Antibodies		
Rabbit anti-GFP	Amsbio	Cat# TP401; RRID: AB_10890443
Rat monoclonal anti-HA	Roche	Cat# 3F10; RRID: AB_2314622
mouse monoclonal anti-HA	Babco	Clone #16B12
Rabbit anti-CP190	Schoborg et al.[56]; Marino Labrador laboratory	N/A
mouse anti-CP190	Schoborg et al.[56]; Marino Labrador laboratory	N/A
rabbit anti-Mod(mdg4)67.2	Schoborg et al.[56]; Marino Labrador laboratory	N/A
rabbit anti-Su(Hw)	Schoborg et al.[56]; Marino Labrador laboratory	N/A
Mouse anti-BEAF-32	DSHB	Cat# anti-BEAF; RRID: AB_1553420
anti-βPS-integrin	DSHB CF.6G11	Cat# cf.6g11; RRID: AB_528310
anti-Futsch	DSHB 22C10	Cat# 22c10; RRID: AB_528403
mouse anti-LaminDm0	DSHB ADL67.10	Cat# adl67.10; RRID: AB_528336
mouse anti-HP1a	DSHB C1A9	DSHB Cat# c1a9; RRID: AB_528276
Rabbit anti-Gelsolin	James and Elgin[90]	N/A
goat anti-mouse IgG Alexa Fluor 488	Molecular Probes	Cat# A-11001; RRID: AB_2534069
goat anti-mouse IgG Alexa Fluor 568	Molecular Probes	Cat# A-11031; RRID: AB_144696
goat anti-rat IgG Alexa Fluor 488	Molecular Probes	Cat# A-11006; RRID: AB_141373
goat anti-rat IgG Alexa Fluor 568	Molecular Probes	Cat# A-11077; RRID: AB_2534121
goat anti-guinea pig IgG Alexa Fluor 488	Molecular Probes	Cat# A-11073; RRID: AB_2534117
goat anti-rabbit IgG Alexa Fluor 488	Molecular Probes	Cat# A-11034; RRID: AB_2576217
goat anti-rabbit IgG Alexa Fluor 568	Molecular Probes	Cat# A-11036; RRID: AB_10563566
goat anti-mouse HRP	Jackson Labs	Cat# 115-035-062; RRID: AB_2338504
GFP nanobody Alexa Fluor 488	Dirk Görlich laboratory	Nanobody-ID SB19
Chemicals, peptides, and recombinant proteins		
VECTASHIELD plus DAPI	Vector	SKU: H-1200-10
VECTASHIELD	Vector	SKU: H-1000-10
phalloidin-rhodamine	Thermo Fisher Scientific	Cat# R415
Schneider medium	Thermo Fisher Scientific	Cat# 21720024
Critical commercial assays		
stain-free precast 4 – 20% SDS-PAGE gels	Bio-Rad	Cat# 4568095
T7-MEGAshortscript Kit	Life Technologies	Cat# AM1354
MEGAclear Transcription Clean-Up Kit	Life Technologies	Cat# AM1908
Superscript III First-Strand Synthesis System	Invitrogen	Cat# 18080–051
Dynabeads	Invitrogen	Cat# 610.06
Deposited data		
RNAseq data	This paper	https://www.ncbi.nlm.nih.gov/geo/query/acc.cgi?acc=GSE270794
Experimental models: Cell lines		
D. melanogaster: Cell line S2: S2-DRSC	Laboratory of Norbert Perrimon	FlyBase: FBtc0000181

(*Continued on next page*)

Continued

REAGENT or RESOURCE	SOURCE	IDENTIFIER
Experimental models: Organisms/strains		
D. melanogaster: w1118	BDSC	RRID: BDSC_3605
D. melanogaster: w1118; Df(3L)ED4502, P{3'.RS5+3.3'}ED4502/TM6C, cu1 Sb1	BDSC	RRID: BDSC_8097
D. melanogaster: tono-GFP Fosmid (fTRG10059)	VDRC	VDRC-ID: 318375
D. melanogaster: 5xUAS-tono-3xHA	FlyORF.ch; Johannes Bischof	N/A
D. melanogaster: Act88F-GAL4	BDSC	RRID: BDSC_99925
D. melanogaster: Mhc[10]	Collier et al.[91]; Sanford Bernstein laboratory	N/A
D. melanogaster: UAS-CD8GFP	BDSC	RRID: BDSC_32184
D. melanogaster: stripe-GAL4	BDSC	RRID: BDSC_26663
D. melanogaster: UAS-mit-GFP	BDSC	RRID: BDSC_25747
D. melanogaster: Mef2-GAL4	BDSC	RRID: BDSC_27390
D. melanogaster: UAS-GFP-Gma	BDSC	RRID: BDSC_31776
D. melanogaster: CTCF[GE24185]	Mohan et al.[59]; Rainer Renkawitz laboratory	N/A
D. melanogaster: CTCF[P30.6]	Mohan et al.[59]; Rainer Renkawitz laboratory	N/A
D. melanogaster: BEAF32[AB-KO]	Roy et al.[92]; Robert J Johnston Jr	N/A
D. melanogaster: CP190[1]	Jordan Raff laboratory	N/A
D. melanogaster: CP190[2]	Jordan Raff laboratory	N/A
D. melanogaster: Talin-C-terminal-YPet	Lemke et al.[93]	N/A
D. melanogaster: tono[1]	This paper	N/A
D. melanogaster: tono[2]	This paper	N/A
D. melanogaster: tono-HA	This paper	N/A
D. melanogaster: Tono-ΔBTB-HA	This paper	N/A
D. melanogaster: Tono-ΔZFs-HA	This paper	N/A
D. melanogaster: LDH-cherry	Krejcova et al.[55]; Jason Tennessen laboratory	N/A
D. melanogaster: *y[1], M(Act5C-Cas9)ZH-2A, w[1118], DNAlig4[169]*	BDSC	RRID: BDSC_58492
Oligonucleotides		
XZ13 Mutation detect primer CG32121(tono) forward : GCCAGGAGAGGGGTGTTAAG	This paper	N/A
XZ14 Mutation detect primer CG32121(tono) reverse : ACCTCTCCGACATCCGACAT	This paper	N/A
sgRNA1: GTGTAATGCGGTGAAAGCG	This paper	N/A
sgRNA2: GGGTCTAAGACGTTGGTTT	This paper	N/A
Software and algorithms		
CRISPRscan	Moreno-Mateos et al.[94]	https://www.crisprscan.org
STAR	Dobin et al.[95]	https://code.google.com/archive/p/rna-star/
RNfuzzyApp	Haaering and Habermann[96]	https://gitlab.com/habermann_lab/rna-seq-analysis-app
FlyEnrichR[97]	Kuleshov et al.[98]	https://maayanlab.cloud/FlyEnrichr/
Fiji (ImageJ)	Schindelin et al.[99]	https://imagej.net/software/fiji/
Fiji macro MyofibrilJ	Spletter et al.[19]	https://imagej.net/plugins/myofibrilj
Prism 9 (version 9.5.1)	GraphPad Software	https://www.graphpad.com
mitoXplorer 2.0	Marchiano et al.[53]	https://mitoxplorer2.ibdm.univ-amu.fr/about.html
Fiji macro granularity score	This paper	https://github.com/PierreMangeol/Tono

RESOURCE AVAILABILITY

Lead contact

Further information and requests for resources and reagents should be directed to and will be fulfilled by the lead contact, Frank Schnorrer (frank.schnorrer@univ-amu.fr).

Materials availability

Unique materials generated in this study are available from the lead contact without restriction.

Data and code availability

- mRNA sequencing data have been deposited at GEO (Gene Expression Omnibus) and are publicly available as of the date of publication. Accession numbers are listed in the key resources table. GEO: GSE270794.
- All original code has been deposited at https://github.com/PierreMangeol/Tono and is publicly available as of the date of publication. DOIs are listed in the key resources table. Any additional information required to reanalyze the data reported in this work paper is available from the lead contact upon request.

EXPERIMENTAL MODEL AND STUDY PARTICIPANT DETAILS

Drosophila husbandry and strains

Fly stocks were maintained and crosses were performed under normal culture conditions in humidified incubators with 12-hour light-dark cycles at 27 °C unless specified. All fly stocks crosses were maintained on standard lab fly medium. The standard lab medium is a variation of the Caltech media recipe, which includes 8% (w/v) cornmeal, 2% (w/v) yeast, 3% (w/v) sucrose, 1,1% (w/v) agar, 1% (v/v) acid mix. To prepare the media, cornmeal (80 g), sucrose (30 g), dry-yeast (20 g) and agar (11 g) were mixed in 1 L of water and brought to boil with constant stirring. The media was allowed to cool down to 60°C, before 10 ml of acid mix was added. Acid mix was prepared by mixing equal volumes of 10% propionic acid (v/v) and 83.6% orthophosphoric acid. The medium was then poured in vials (~10 ml/vial) or bottles (50 ml/bottle) and allowed to cool down before storing at 4°C for later usage.

The *CG32121* deficiency line (*w[1118]; Df(3L)ED4502, P{3'.RS5+3.3'}ED4502/TM6C, cu*^{1} *Sb*^{1}) was obtained from the Bloomington Drosophila stock center (BDSC). *tono-GFP* Fosmid (fTRG10059) was generated within the FlyFos collection.[46] In the rescue experiments, *tono-GFP* Fosmid was recombined with *tono[1]* or *tono[2]* and the recombinant was identified by PCR. Tissue-specific rescue was performed at 18°C by driven UAS-*tono-HA* (obtained from Johannes Bischof[100]) with the flight muscle-specific driver *Act88F*-GAL4[101] in the *tono[1]* or *tono[2]* background. Hypercontraction rescue was performed with *Mhc[10]; tono[1] or Mhc[10]; tono[2]* flies by using the flight muscle-specific myosin splicing mutant *Mhc[10]*.[91] Tendon cell labelling was performed by crossing UAS-CD8GFP with *stripe*-GAL4[102] as control or UAS-CD8GFP; *tono[1]* with *tono[1]*, *stripe*-GAL4. Mitochondria were labelled by expressing a fluorescent protein (FP) fused to a mitochondria matrix peptide (mit-GFP).[34] The indirect flight muscles were labelled with *Mef2*-GAL4; UAS-GFP-Gma to facilitate the muscle dissection transcriptomics. Both *CTCF[GE24185]* and *CTCF[P30.6]* (from Rainer Renkawitz)[59] are strong alleles for *CTCF*. *BEAF-32[AB-KO]*[92] (from Robert J Johnston Jr) is a null allele for both *BEAF-32A* and *BEAF-32B*. *CP190[1]* and *CP190[2]*[103] were obtained from Jordan Raff. Live muscle twitching movies were recorded by labelling the muscle ends with Talin-C-terminal-YPet[93] (see below).

METHOD DETAILS

Generation of tono[1] and tono[2] alleles

tono[1] was generated as described with the published TALEN method.[44] Two pairs of TALENs (pair 1 targeting AACCG CAGCATCATC in the first coding exon of *tono* and pair 2 targeting ACTCCGGAGAGGTGA in the second coding exon of *tono*) were designed and constructed.[104] *In vitro* transcribed TALEN mRNAs were injected into *w[1118]* fly embryos at a concentration of 250 ng/μl each. The genomic region covering both targeted sites has been amplified by PCR with primer XZ13 and XZ14 and then followed by a T7 assay to identify successful targeting.[44] Fly stocks with mutations in *tono* were established and sequenced.

tono[2] was constructed by CRISPR-RMCE genome editing as published with small optimisations.[45] An intron sequence between coding exons 1 and 2 of *tono* and a sequence at the end of 3′-UTR of *tono* were chosen for sgRNA designing with CRISPRscan.[94] Four sgRNAs were picked for each targeting region according to the score from CRISPRscan and their activities were estimated in S2 cells.[45] sgRNA 1 (targeting sequences GTGTAATGCGGTGAAAGCG in the intron region) and sgRNA 2 (targeting sequences GGGTCTAAGACGTTGGTTT in 3'-UTR) were picked for embryo injection. The left homology arm of ~2kb and the right arm of ~2kb were assembled with a dsRed cassette as a repair donor.[45] *y[1], M(Act5C-Cas9)ZH-2A, w[1118], DNAlig4[169]* embryos were injected with donor plasmid at 800 ng/μl and sgRNAs at 272 ng/μl each. F1 flies with red fluorescent eyes were chosen for characterization by PCR and sequencing to confirm the cassette insertion. Fly stocks with correct insertion were established as *tono*[2]. For the RMCE exchange, a full length of *tono* coding sequences (CDS), *tono-ΔBTB*, and *tono-ΔZFs* were tagged with 2xHA and

cloned.[45] The plasmids were injected into *tono[2]* fly embryos and the progeny were screened for non-fluorescent eyes and characterized by PCR and sequencing.[45]

Transcriptomics

For transcriptomics, flight muscles from wildtype control and *tono[1]* flies were dissected at either 30 h APF or 48 h APF and isolated based on *Mef2*-GAL4, UAS-GFP-Gma expression.[24] Three replicates were used and each replicate contained indirect flight muscles dissected from 150 pupae. Poly(A)+mRNA was purified using Dynabeads (#610.06, Invitrogen) and integrity was verified on a Bioanalyzer. mRNA was then fragmented by heating to 94 °C for 210 s in fragmentation buffer (40 mM TrisOAc, 100 mM KOAc, 30 mM MgOAc2). First-strand cDNA synthesis was performed with the Superscript III First-Strand Synthesis System (#18080–051, Invitrogen) using random hexamers. The second strand was synthesized with dUTP and libraries were sequenced on an Illumina HiSeq 2500 and multiplexed 3-4 samples per lane, obtaining ~100 million reads per library. Sequencing was performed at the Vienna Biocenter Core Facility (https://www.viennabiocenter.org/vbcf). Reads were filtered and trimmed using the FASTX Toolkit and cutadapt then mapped to the Flybase 2015_04 genome assembly using STAR.[95] Reads were visualized on the UCSC genome browser by normalizing them to the largest library size. featureCounts v1.4.2[105] was used for determining raw read counts. Differential expression analysis was done using the RNfuzzyApp,[96] with the TCC normalization[106] and DESeq2[97] method. Additional data processing was handled in R (see Data S2 for raw, normalized and differential mRNA-Seq data and enrichment analysis).

Phasik analysis

Phasik was used for mitochondrial phase detection.[52] We used the mito-interactome from mitoXplorer 2.0[53] as network, together with the transcriptomic data from the flight muscle developmental time-course[19] to construct the temporal network. We used Euclidian distance and hierarchical clustering with the 'Ward' method for temporal network clustering. As Phasik can detect at multiple scales, we chose to analyze the three main clusters, which reflect the prominent switch between 30 h and 48 h APF in the distance matrix, and a second switch between 72 h and 90 h AFP. An edge weight of 0.7 was chosen to select significant genes for enrichment analysis in the different phases, which was then done with FlyEnrichR[98] (see Data S3 for more information).

Immunostaining and processing

Flight muscle dissections were performed with a slightly modified published protocol.[107] After removing the pupal case from the staged pupae, two to three holes were pinned in the abdomen with insect pins. The samples were then transferred to 4% PFA in PBST (0.5% Triton-X in PBS) and fixed for 20 min at room temperature (RT) on a rocking platform. Samples were transferred to a silicon-coated petri dish and their position was fixed with insect pins.[107] One hole was cut from the head to the abdomen along the ventral middle line. Other tissues in between the two thorax halves were removed by forceps or by pipetting. The two thorax halves were then cut off and transferred to a 24-well plate. The samples were washed with 3x PBST for 10 min each at RT before blocking with 5% normal goat serum (NGS) in PBST for 1 hour at RT. Afterwards, they were incubated with primary antibodies at 4°C overnight and washed 3x in PBST (10 min each) at RT. Incubation with secondary antibodies was performed at room temperature for 2 hours. The samples were washed 3x in PBST and mounted in VECTASHIELD plus DAPI (Vector) to visualize nuclei. The samples were stored at 4°C before imaging. Images were acquired on Zeiss LSM780 or LSM880 confocal with AiryScan and processed with Fiji (ImageJ).[99]

To stain for Su(Hw) and Mod(mdg4)67.2, the samples were dissected and then incubated for 30 min in PBS or PBS + 250mM NaCl before fixing with methanol. The fixation was done in precooled 100% methanol at -20 ºC for 15 min with gentle rocking every 5 min. Afterwards, an equal volume of PBST was added and samples were washed as described above before proceeding to immunostaining.

Heart muscle: head and wings of adult flies were removed with scissors, and the adult fly was pined at thorax level on its back with 2 needles at the bottom of a PBS-filled petri dish. The ventral side of the abdomen was removed by cutting both sides with scissors, starting at the tip of the abdomen towards the thorax. The contents of the abdomen were removed with forceps, with the exception of the heart tube, which remained attached to the dorsal side of the abdomen. Once the heart was exposed, the thorax was cut off and the abdomen was fixed in 4% PFA for 20 minutes and stained as described above for flight muscles. The heart attached to the abdomen was mounted between a slide and a coverslip without spacer.

Jump muscle: fixed thoraces were each cut in two sagittally using a microtome blade. Different to the flight muscle preparation, for jump muscle stainings the thorax was not cut at the middle but asymmetrically at more than three-quarters to expose laterally located jump muscle. The samples were then stained as for the flight muscles and mounted between a slide and a coverslip with one coverslip as a spacer.

Rabbit anti-GFP (1:2000) was obtained from Amsbio (TP401). Rat monoclonal anti-HA (3F10) and mouse monoclonal anti-HA (16B12) were used at 1:500. Rabbit anti-CP190 (dilution 1:2000), mouse anti-CP190 (dilution 1:1000), rabbit anti-Mod(mdg4)67.2 (dilution 1:1000) and rabbit anti-Su(Hw) (1:1000) were gifts from Mariano Labrador.[56] Mouse anti-BEAF-32 (dilution 1:20),[108] mouse anti-βPS-integrin (CF.6G11, dilution 1:100),[109] mouse anti-Futsch (22C10, dilution 1:100),[110] mouse anti-LaminDm0 (ADL67.10, dilution 1:50),[111] and mouse anti-HP1a (C19A, 1:100)[90] were obtained from DSHB. Rabbit anti-Gelsolin (dilution, 1:2000)[112] was a gift from Maria Leptin. All the primary antibodies were diluted in PBST with 5% NGS. All the secondary antibodies, including goat anti-mouse, goat anti-rat, goat anti-pig, and goat anti-rabbit, and phalloidin-rhodamine were purchased from Molecular Probes and applied at 1:500 dilution. Tono-GFP signal was boosted after fixation with a GFP nanobody (gift of Dirk Görlich) at 1:2000 for 2 hours at room temperature.

Osmotic and mechanical manipulations

To induce hyper-osmotic stress, correctly staged pupae were taken out of their pupal case using forces. Dissection needles were used to pierce three small holes into the abdomen of the pupae, which were then incubated in PBS control or PBS + 250 mM NaCl or PBS + 500 mM sucrose at RT for 30 min under gentle agitation. Then pupae were fixed and flight muscles were dissected, stained and visualized as described above. The reversibility of the Tono droplets was tested by first treating the living pupae with PBS + 250 mM NaCl or PBS control for 20 min and then followed by a hypo-osmotic 0.1x PBS treatment or PBS control for another 20 min. Then pupae were fixed and flight muscles were stained as described above.

Mechanical manipulations were performed by preparing living adult hemi-thoraxes from Tono-GFP flies, without damaging the flight muscles[34] and mounting them between a slide and a coverslip using either 4 or 2 layers of Scotch tape on each side as spacer for the relaxed or squeezed conditions, respectively. The flight muscles were imaged within the next 20 minutes after the dissection.

To image the dynamics of Tono-GFP at high time resolution, living intact flight muscles were mounted the same way as above for the mechanical manipulation, this time with 2 layers of Scotch tape. The muscles were imaged immediately after manually squeezing the sample by pressing on the coverslip. Samples were imaged with a spinning disc confocal within 1 minute after pressing on the coverslip.

Spontaneous contractions

To image muscle twitching at pupal stages, we used Talin-C-terminal-YPet[19,113]: prior to imaging, a window was cut in the pupal case and pupae were mounted in custom slotted slides with the window in the pupal case above pupal thorax facing up. The hole was covered with 50% glycerol and a coverslip. Live imaging of developmental spontaneous contractions was performed on a Leica SP5 confocal microscope. At the specified developmental time point, flight muscle attachment sites labelled with Talin-YPet were recorded every 0.65 seconds for 5 min. General movement within the thorax was distinguished from IFM-specific contractions, and each sample was scored for the number of single or double contractions observed per 5-minute time window. Data were recorded in Excel and ANOVA was performed in GraphPad Prism to determine significant differences. Movies were assembled in Fiji, cropped and edited for length to highlight a selected twitch event.

Behavioral tests

Flight tests were performed as previously described[93]: around 20-30 fresh adult males (1-3 days after eclosion) were collected and recovered for 48 hours in the incubator at 27 degrees. Flies were introduced into a flight test cylinder divided into 3 zones and the landing position of the flies was documented.

Jump tests were performed with one-week-old *white[1118]* or *tono[2]* males. Adults were anaesthetized with CO_2, males were sorted and their wings were clipped with scissors. They were allowed to recover for 48 h in the incubator. The jump test was performed in a petri dish equipped with millimeter paper and filmed by a camera. Flies were tested individually and stimulated by manual touch with a brush until 5 jumps were for each fly obtained. The length of the five jumps was averaged to obtain one value for each fly. 10 *white[1118]* and 11 *tono[2]* flies were tested.

Locomotion (geotaxis) tests were performed in empty fly tubes containing 20 young males that were sorted at least 24 hours before. The flies were banged to the bottom of the tube and their positions were recorded 10 seconds later. Depending if the flies crossed a line drawn at 7 centimeters from the bottom, they were counted as in the top or bottom fraction. Each cohort of 20 flies was tested 4 times for climbing and the percentage of flies in the bottom or top section was obtained by averaging the 4 tests. 6 cohorts of *white[1118]* or *tono[2]* flies were tested.

Western blotting

Each adult thorax protein extract was made from 10 adult fly thoraxes (head, wings and abdomen removed by scissors) that were homogenized in 200 µl 6x Laemmli buffer (375 mM Tris-HCl pH 6.8, 9% SDS, 50% glycerol, 0.03% bromophenol blue), boiled for 3 min and stored at -20°C. 5µl were loaded per lane on stain-free precast 4 – 20% SDS-PAGE gels (Bio-Rad). Western blots were performed using Bio-Rad blotting chambers under standard conditions.[7] Total protein load after membrane transfer was obtained by imaging the PVDF membranes using the stain-free protocol. HA-tagged proteins were revealed by incubating the membrane, after blocking with milk for 1 h, with mouse monoclonal anti-HA (16B12 at 1:10 000 overnight at 4 °C), followed by and goat anti-mouse HRP (1:10 000 for 2 hrs at RT), followed by ECL incubation and chemiluminescence camera detection. For each genotype (*white[1118]*, *tono-HA*, *tono-ΔZFs-HA*, *tono-ΔBTB-HA*) four independent biological samples were made and blotted. HA-band intensities were related to total protein load using the stain-free membrane quantification in the region of interest. Relative Tono-HA levels on each blot were set to 1.

QUANTIFICATION AND STATISTICAL ANALYSIS

Sarcomere length quantification

The flight muscles were stained with rhodamine phalloidin and images were acquired with a Leica LSM780 or LSM880 confocal. Sarcomere length was measured using the Fiji plug-in MyofibrilJ.[19] Two-tailed unpaired student t-tests were performed between wild type and *tono[1]* or *tono*[2]. Error bars represent the standard deviation.

Mitochondria aspect and area quantifications

Mitochondria were labelled by expressing mitochondrial matrix-directed GFP (UAS-mitGFP, BDSC: 25747). Quantification of the aspect ratio (length/width) of the mitochondria was performed in a double-blind fashion using hand segmentation, systematically measuring the long and short axes of each mitochondrion from a cropped image of 40 μm x 20 μm. Mitochondria were quantified from n>4 thoraxes. The total area of mitochondria is identified by Otsu thresholding on Fiji for each z-plane. The multiple quantifications for each z-plane were averaged for each animal (one value per animal).[34]

Tono-granularity quantification

To quantify the Tono granularity score, each nucleus was segmented in 2D in one z-plane. For each nucleus (ROI) the mean signal and its standard deviation were retrieved to quantify the granularity score (mean/std) using a Fiji macro (https://github.com/PierreMangeol/Tono). The granularity score of all nuclei segmented from one pupa was averaged to calculate one value per animal. To verify our methodology, we devised a simple simulation in Python to mimic the different images of Tono condensation states we observed. We then quantified these images the same way we analyzed Tono distributions in the muscle nuclei. In this simulation, the total amount of Tono is constant, and at a given state of condensation, Tono condensates are spheres of equal radii that cannot overlap each other. Spheres spread over a two-dimensional square area that is the same for the entire simulation. To simulate images of these condensates, images of these spheres were simplified as discs, and to take into account the diffraction-limited nature of microscopy observations, images were convoluted with a Gaussian kernel. The resulting simulated images are comparable to real microscopy images that would be obtained with a resolution of 210 nm (wavelength of 550 nm observed with an objective of N.A. 1.3) and particle diameters ranging from 100 nm to 700 nm. This simulation is an oversimplification of reality, but it recapitulates well the fact that the mean-normalized standard deviation of intensity of Tono in nuclei increases together with the condensation process (Figure S8).

Nuclear aspect ratio quantification

Muscle samples stained with anti-Lamin antibody were used to determine the nuclear aspect ratio. To quantify the nuclear aspect ratio (length/width), the long and short axes of each nucleus present in one z-plane were retrieved. The aspect ratios of all nuclei in the z-plane were averaged to calculate one value per animal. The ratio for each muscle type and developmental time point was quantified from 5 animals.

Statistical analysis

Quantification and statistical analysis are reported in Data S1. The box and whisker plot represent the median, 25th and 75th percentiles for the box, and the minimum and maximum values for the whiskers. Bar plot represent the mean and the standard deviation. n stands for the number of animals, unless otherwise stated in the legend. Unpaired t-tests were performed in GraphPad Prism 8.0.2. Ns: $P > 0.05$; *: $P \leq 0.05$; **: $P \leq 0.0$; ***: $P \leq 0.001$; **** $P \leq 0.0001$.